

1  
2  
3  
4  
5  
6  
7  
8  
9  
10

---

This manuscript has been submitted for publication in RAPID COMMUNICATIONS IN MASS SPECTROMETRY. A newer version of this preprint is available on Authorea (<https://doi.org/10.22541/au.167458072.24405970/v2>). Please note that, despite having undergone peer-review, the manuscript has yet to be formally accepted. Subsequent versions of this manuscript may have slightly different content. If accepted, the final version of this manuscript will be available via the '*Peer-reviewed Publication DOI*' link on the right-hand side of this webpage. Please feel free to contact us — we welcome feedback.

---

11 In preparation for Rapid Communications in Mass Spectrometry  
12 **pyisotopomer: A Python package for obtaining intramolecular isotope ratio differences**  
13 **from mass spectrometric analysis of nitrous oxide isotopocules**  
14 Colette L. Kelly,<sup>1\*</sup> Cara Manning,<sup>2</sup> Claudia Frey,<sup>3</sup> Jan Kaiser,<sup>4</sup> Noah Gluschkoff,<sup>1</sup> and Karen  
15 L. Casciotti

- 16 1. Stanford University, Department of Earth System Science, Stanford, CA 94305, USA  
17 2. University of Connecticut, Department of Marine Sciences, Groton, CT, 06340, USA  
18 3. Department of Environmental Science, University of Basel, Basel, Switzerland.  
19 4. University of East Anglia, Centre for Ocean and Atmospheric Sciences, School of  
20 Environmental Sciences, Norwich, NR4 7TJ, UK

21  
22 \* **Correspondence to:** Colette L. Kelly (email: [clkelly@stanford.edu](mailto:clkelly@stanford.edu); phone: 802-595-3647;  
23 address: 473 Via Ortega Room 140, Stanford, CA 94305).

24  
25 **Keywords:** Nitrous oxide, isotopomers, isotopocules, scrambling, Python

26  
27 **Abstract**

28  
29 **RATIONALE** Obtaining nitrous oxide isotopocule measurements with isotope ratio mass  
30 spectrometry (IRMS) involves analyzing the ion current ratios of the nitrous oxide parent ion  
31 ( $\text{N}_2\text{O}^+$ ) as well as those of the  $\text{NO}^+$  fragment ion. The data analysis requires correcting for  
32 “scrambling” in the ion source, whereby the  $\text{NO}^+$  fragment ion obtains the outer N atom from the  
33  $\text{N}_2\text{O}$  molecule. While descriptions exist for this correction, and interlaboratory intercalibration  
34 efforts have been made, there has yet to be published a package of code for implementing  
35 isotopomer calibrations.

36  
37 **METHODS** We developed a user-friendly Python package (pyisotopomer) to determine two  
38 coefficients ( $\gamma$  and  $\kappa$ ) that describe scrambling in the IRMS ion source, and then to use this  
39 calibration to obtain intramolecular isotope deltas in  $\text{N}_2\text{O}$  samples.

40  
41 **RESULTS** With two appropriate reference materials,  $\gamma$  and  $\kappa$  can be determined robustly and  
42 accurately for a given IRMS. An additional third reference material is needed to define the zero-  
43 point of the delta scale. We show that IRMS scrambling behavior can vary with time,  
44 necessitating regular calibrations. Finally, we present an intercalibration between two IRMS  
45 laboratories, using pyisotopomer to calculate  $\gamma$  and  $\kappa$ , and to obtain intramolecular  $\text{N}_2\text{O}$  isotope  
46 deltas in lake water unknowns.

47  
48 **CONCLUSIONS** Given these considerations, we discuss how to use pyisotopomer to obtain  
49 high-quality  $\text{N}_2\text{O}$  isotopocule data from IRMS systems, including the use of appropriate  
50 reference materials and frequency of calibration.

## 51 1. Introduction

52 Nitrous oxide (N<sub>2</sub>O) is a potent greenhouse gas, with a global warming potential 265  
53 times that of carbon dioxide over a 100 year time horizon<sup>1,2</sup>. N<sub>2</sub>O is also likely to be the most  
54 emitted ozone depletion agent in the 21<sup>st</sup> century, due to production of NO radicals in the  
55 stratosphere that interact destructively with ozone<sup>3-6</sup>. Historically, the bulk stable isotopes of  
56 nitrogen and oxygen in N<sub>2</sub>O have been used to quantify its microbial cycling in soils<sup>7,8</sup> and in the  
57 ocean<sup>9-12</sup>, its destruction by photolysis and O(<sup>1</sup>D), and its cycling in the atmosphere<sup>13,14</sup>. This  
58 approach often fails at disentangling different N<sub>2</sub>O production and consumption mechanisms,  
59 because the bulk nitrogen and oxygen isotope ratios of N<sub>2</sub>O depend on the isotopic composition  
60 of the substrate, as well as the isotope effects of production and consumption processes<sup>12</sup>.  
61 Furthermore, in the context of microbial N<sub>2</sub>O cycling in soils and the ocean, bacterial  
62 nitrification and denitrification produce N<sub>2</sub>O with similar bulk  $\delta(^{15}\text{N})$ <sup>1</sup> values, preventing  
63 partitioning between these processes on the basis of bulk  $\delta(^{15}\text{N})$  alone<sup>15,16</sup>.

64 The site-specific nitrogen isotope ratios of N<sub>2</sub>O provide a more nuanced constraint on the  
65 biogeochemical cycling of N<sub>2</sub>O than its bulk composition alone. N<sub>2</sub>O isotopomers have been  
66 used extensively to quantify its biogeochemical cycling in soils<sup>17-20</sup>, the atmosphere<sup>14,21-23</sup>, and  
67 the ocean<sup>24-34</sup>. The individual isotopic compositions of each nitrogen atom were first measured  
68 by Friedman and Bigeleisen, who quantified the yields of isotopomers <sup>14</sup>N<sup>15</sup>N<sup>16</sup>O and <sup>15</sup>N<sup>14</sup>N<sup>16</sup>O  
69 from enriched ammonium nitrate by measuring the NO<sup>+</sup> fragment ion signal in an isotope ratio  
70 mass spectrometer (IRMS)<sup>35</sup>. 50 years later, these N<sub>2</sub>O isotopomers were quantified at natural  
71 abundance from the N<sub>2</sub>O<sup>+</sup> species with mass numbers 44, 45, and 46 and the mass 30 and 31  
72 NO<sup>+</sup> fragment ion<sup>36,37</sup>. The central nitrogen atom in the N<sub>2</sub>O molecule has been designated with  
73 locants  $\alpha$ ,  $\mu$ , or 2; the terminal atom, with locants  $\beta$ ,  $\tau$ , or 1<sup>38,39</sup>. Here, we use the definitions from  
74 Toyoda and Yoshida (1999) for the site-specific isotope number (N) ratios of the central ( $\alpha$ )  
75 nitrogen atom and terminal ( $\beta$ ) nitrogen atom<sup>36</sup>:

$$^{15}R^{\alpha} = \frac{N(^{14}\text{N}^{15}\text{NO})}{N(^{14}\text{N}^{14}\text{NO})} \quad (1)$$

76

$$^{15}R^{\beta} = \frac{N(^{15}\text{N}^{14}\text{NO})}{N(^{14}\text{N}^{14}\text{NO})} \quad (2)$$

77

78 The N<sub>2</sub>O isotopomer measurement was initially performed with two sequential  
79 measurements of the same sample on an isotope ratio mass spectrometer, one at  $m/z$  44, 45, and  
80 46, and the other at  $m/z$  30 and 31<sup>36</sup>. Use of dedicated cup-configurations on lower-dispersion  
81 IRMS instruments allowed simultaneous analysis of all five masses together<sup>40</sup>.

82 The slight difference in absorption cross sections between the isotopocules of N<sub>2</sub>O result  
83 in different isotopic fractionations during photolysis and photo-oxidation in the stratosphere<sup>41</sup>,  
84 making the isotopomers of N<sub>2</sub>O a powerful tool for understanding its atmospheric cycling<sup>21,42-45</sup>.  
85 Likewise, N<sub>2</sub>O site preference, defined as  $\delta(^{15}\text{N}^{\text{sp}}) = \delta(^{15}\text{N}^{\alpha}) - \delta(^{15}\text{N}^{\beta})$ , was shown in microbial  
86 culture experiments to be largely a function of reaction mechanism, independent of source  
87 composition<sup>24,46-50</sup>. This allowed for the differentiation between N<sub>2</sub>O from bacterial nitrification  
88 ( $\delta(^{15}\text{N}^{\text{sp}}) \approx 28-38$  ‰) and denitrification ( $\delta(^{15}\text{N}^{\text{sp}}) \approx 0$ )<sup>24,46-50</sup>, although more studies are needed  
89 to better constrain the SPs for diverse fungal, bacterial, and archaeal strains in both terrestrial and

---

<sup>1</sup> We write  $\delta$  values with parentheses, e.g.,  $\delta(^{15}\text{N})$ , because  $\delta$  is the quantity symbol and “<sup>15</sup>N” is the label. See SI Brochure: <https://www.bipm.org/en/publications/si-brochure/>

90 marine environments<sup>49,51</sup>. During N<sub>2</sub>O consumption,  $\delta(^{15}\text{N}^\alpha)$  and  $\delta(^{18}\text{O})$  were shown in microbial  
 91 culture<sup>52</sup> and soil mesocosm<sup>19</sup> experiments to exhibit a characteristic relationship, allowing  
 92 subsequent studies to use this relationship to distinguish between oxidative and reductive  
 93 regimes of N<sub>2</sub>O cycling<sup>30,33</sup>.

94 Site-specific nitrogen isotope ratio measurements based on mass spectrometry need to be  
 95 corrected for a phenomenon called “scrambling,” whereby the NO<sup>+</sup> fragment ion contains the  
 96 terminal N atom, rather than the central N attached to the O atom (as in the original molecule). A  
 97 number of approaches have been taken to calibrate an IRMS system for this effect: 1) the use of  
 98 a single “rearrangement factor” to describe scrambling<sup>36,53</sup>, 2) the use of nine coefficients to  
 99 describe the different fragmentation behaviors of the different isotopocules of N<sub>2</sub>O<sup>54</sup>, and finally  
 100 3) the use of two coefficients to describe scrambling in the ion source<sup>50</sup>. While descriptions exist  
 101 for each of these approaches, and interlaboratory intercalibration efforts have been made<sup>55,56</sup>,  
 102 there has yet to be published a package of code for implementing any of the above isotopomer  
 103 calibrations.

104 We developed a Python software package (“pyisotopomer”) that implements the two-  
 105 coefficient approach described by Frame and Casciotti<sup>32</sup> to calibrate an IRMS for scrambling and  
 106 use that calibration to obtain high-quality N<sub>2</sub>O isotopocule data. This software solves a set of  
 107 equations, either analytically or with an optimization routine, to quantify the scrambling behavior  
 108 of an IRMS. To quantify the performance of the software, we tested the sensitivity of the  
 109 analytical and optimization-based solutions to their input conditions and assessed when each  
 110 method is most appropriate. To quantify the variability of the fragmentation behavior of an  
 111 instrument over time, we examined the scrambling behavior of one IRMS over the course of four  
 112 years of measurements. We derived a simplified equation and used a Monte Carlo simulation  
 113 approach to quantify the effect of uncertainty in the scrambling coefficients on the final isotope  
 114 deltas. Finally, we performed an intercalibration using this software across two labs, at Stanford  
 115 University (‘Lab 1’) and the University of Basel (‘Lab 2’). This paper introduces the theory,  
 116 practical applications, and testing of pyisotopomer; instructions on how to use pyisotopomer are  
 117 available in the documentation on the Python Package Index<sup>57</sup>.

## 119 2. Mathematical framework

120 The molecular ion number ratios 45/44 (<sup>45</sup>R) and 46/44 (<sup>46</sup>R) can be written in terms of  
 121 atomic isotope ratios as<sup>36,53</sup>:

$$^{45}R = ^{15}R^\alpha + ^{15}R^\beta + ^{17}R \quad (3)$$

$$^{46}R = (^{15}R^\alpha + ^{15}R^\beta)^{17}R + ^{18}R + ^{15}R^\alpha ^{15}R^\beta \quad (4)$$

122 where <sup>15</sup>R<sup>α</sup>, <sup>15</sup>R<sup>β</sup>, <sup>17</sup>R and <sup>18</sup>R denote the number ratios of <sup>14</sup>N<sup>15</sup>N<sup>16</sup>O, <sup>15</sup>N<sup>14</sup>N<sup>16</sup>O, <sup>14</sup>N<sub>2</sub><sup>17</sup>O, and  
 123 <sup>14</sup>N<sub>2</sub><sup>18</sup>O, respectively, to <sup>14</sup>N<sub>2</sub><sup>16</sup>O, assuming a stochastic isotope distribution between mono- and  
 124 poly-substituted isotopocules.

125 For many N<sub>2</sub>O samples, <sup>17</sup>R covaries with <sup>18</sup>R according to the oxygen isotope ratios of  
 126 Vienna Standard Mean Ocean Water (VSMOW)<sup>58,59</sup> and a mass-dependent relationship between  
 127 <sup>17</sup>R and <sup>18</sup>R with coefficient  $\beta = 0.516$ <sup>60</sup>. Deviations from this relationship are expressed by the  
 128 oxygen triple isotope excess  $\Delta(^{17}\text{O})$ <sup>60-62</sup>, which provides additional information about the sources  
 129 and sinks of N<sub>2</sub>O<sup>60,63</sup>:

$$^{17}R/^{17}R_{\text{VSMOW}} = (^{18}R/0.0020052)^\beta [\Delta(^{17}\text{O}) + 1] \quad (5)$$

130  $\Delta(^{17}\text{O})$  is sometimes assumed to be equal to zero but should be measured separately for  
 131 samples with a significant  $\Delta(^{17}\text{O})$  anomaly, such as atmospheric nitrate<sup>60,62,63</sup>.

132 The simplest formulation for the  $\text{NO}^+$  fragment ion number ratio 31/30 ( $^{31}R$ ) is given as<sup>36</sup>:  

$$^{31}R = ^{15}R^\alpha + ^{17}R \quad (6)$$

133 This equation would represent the  $^{31}R$  measured by IRMS if no scrambling occurred.

134 To describe instead the scrambled  $^{31}R$ , Toyoda and Yoshida<sup>36</sup> define the rearrangement  
 135 factor  $\gamma$  (which was later given the symbol  $\gamma$ ) as “the fraction of  $\text{NO}^+$  bearing the  $\beta$  nitrogen of  
 136 the initial  $\text{N}_2\text{O}$  to the total  $\text{NO}^+$  formed,” to yield:

$$^{31}R = (1 - \gamma)^{15}R^\alpha + \gamma^{15}R^\beta + ^{17}R \quad (7)$$

137 where  $^{15}R^\alpha$  and  $^{15}R^\beta$  represent atomic isotope ratios of the sample. In other words,  $\gamma$  relates the  
 138 scrambled  $\text{NO}^+$  fragment ratio to the unscrambled  $^{15}R^\alpha$  and  $^{15}R^\beta$  of the sample.

139 Kaiser et al.<sup>53</sup> introduced a more complete representation of  $^{31}R$ , adding terms for  
 140  $^{15}\text{N}^{15}\text{N}^{16}\text{O}$ ,  $^{14}\text{N}^{15}\text{N}^{17}\text{O}$ , and  $^{15}\text{N}^{14}\text{N}^{17}\text{O}$  to  $m/z$  31, and terms for  $^{15}\text{N}^{14}\text{N}^{16}\text{O}$  and  $^{14}\text{N}^{15}\text{N}^{16}\text{O}$  to  $m/z$   
 141 30:

$$\begin{aligned} ^{31}R &= (1 - \gamma)^{15}R^\alpha + \gamma^{15}R^\beta + ^{17}R - \frac{\gamma(1 - \gamma)(^{15}R^\alpha - ^{15}R^\beta)^2}{1 + \gamma^{15}R^\alpha + (1 - \gamma)^{15}R^\beta} \quad (8) \\ &= \frac{(1 - \gamma)^{15}R^\alpha + \gamma^{15}R^\beta + ^{15}R^\alpha^{15}R^\beta + ^{17}R[1 + \gamma^{15}R^\alpha + (1 - \gamma)^{15}R^\beta]}{1 + \gamma^{15}R^\alpha + (1 - \gamma)^{15}R^\beta} \end{aligned}$$

142 Note that Kaiser et al.<sup>53</sup> use the symbol “ $s$ ” for  $\gamma$ ,  $^{15}R_1$  for  $^{15}R^\beta$ , and  $^{15}R_2$  for  $^{15}R^\alpha$ .

143 To account for different fragmentation rates of different  $\text{N}_2\text{O}$  isotopocules, Westley et  
 144 al.<sup>54</sup> replaced the rearrangement factor  $\gamma$  with nine separate coefficients:

$$^{31}R = \frac{a_{31}^{15}R^\alpha + b_{31}^{15}R^\beta + c_{31}^{15}R^\alpha^{15}R^\beta + ^{17}R[d_{31} + e_{31}^{15}R^\alpha + f_{31}^{15}R^\beta]}{1 + a_{30}^{15}R^\alpha + b_{30}^{15}R^\beta + c_{30}^{15}R^\alpha^{15}R^\beta} \quad (9)$$

145 While this approach considers the possibility of different rearrangement factors for every  
 146  $\text{N}_2\text{O}$  isotopocule as well as  $^{15}\text{N}_2^+$  formation, it also requires solving for three to nine coefficients,  
 147 depending on whether  $a_{30}$ ,  $b_{30}$  and  $c_{30}$ , as well as  $d_{31}$ ,  $e_{31}$  and  $f_{31}$ , are considered separately from  
 148 coefficients  $a_{31}$ ,  $b_{31}$  and  $c_{31}$ .

149 Frame and Casciotti<sup>50</sup> simplify this equation by reducing the number of rearrangement  
 150 factors to two coefficients,  $\gamma$  and  $\kappa$ , which represent the yield of  $^{14}\text{NO}^+$  from  $^{14}\text{N}^{15}\text{N}^{16}\text{O}$  and  
 151  $^{14}\text{N}^{15}\text{N}^{17}\text{O}$ , and the yield of  $^{15}\text{NO}^+$  from  $^{15}\text{N}^{14}\text{N}^{16}\text{O}$ , respectively. This produces the equation:

$$^{31}R = \frac{(1 - \gamma)^{15}R^\alpha + \kappa^{15}R^\beta + ^{15}R^\alpha^{15}R^\beta + ^{17}R[1 + \gamma^{15}R^\alpha + (1 - \kappa)^{15}R^\beta]}{1 + \gamma^{15}R^\alpha + (1 - \kappa)^{15}R^\beta} \quad (10)$$

153 The important pieces of information contained within the two scrambling factors are the  
 154 unequal rates of fragmentation for the isotopomers  $^{14}\text{N}^{15}\text{NO}$  and  $^{15}\text{N}^{14}\text{NO}$ , which eqns. (7) and  
 155 (8) assume are equal. Eqn. (10) is formulated by assuming that the  $^{17}\text{O}$ -isotopocules have the  
 156 same scrambling behavior as the  $^{16}\text{O}$ -isotopocules, i.e.,  $e_{31} = 1 - a_{31}$  and  $f_{31} = 1 - b_{31}$ , in terms of  
 157 the coefficients in eqn. (9). It is also assumed that  $c_{31} = 1$ , i.e., the yield of  $^{15}\text{N}^{16}\text{O}^+$  from  $^{15}\text{N}_2^{16}\text{O}$   
 158 is equal to the yield of  $^{14}\text{N}^{16}\text{O}^+$  from  $^{14}\text{N}_2^{16}\text{O}$ . Given that naturally occurring  $\text{N}_2\text{O}$  contains very  
 159 little  $^{15}\text{N}_2^{16}\text{O}$ , a small difference in this yield would not significantly alter  $^{31}R$ <sup>64</sup>. Finally, it is  
 160 assumed that  $d_{31} = 1$ , or that the yield of  $^{14}\text{N}^{17}\text{O}^+$  from  $^{14}\text{N}_2^{17}\text{O}$  is equal to the yield of  $^{14}\text{N}^{16}\text{O}^+$   
 161 from  $^{14}\text{N}_2^{16}\text{O}$ ; again, an assumption yielding little error in  $^{31}R$ , given the low natural abundance  
 162 of  $^{17}\text{O}$  in  $\text{N}_2\text{O}$ <sup>60</sup>.

163 Eqn. (10) can be rearranged to give an equation for  $\gamma$  as a function of  $\kappa$  (the full derivation  
164 is presented in Supplementary text S1):

$$\gamma = \frac{{}^{15}R^\alpha + \kappa {}^{15}R^\beta + {}^{15}R^\alpha {}^{15}R^\beta - ({}^{31}R - {}^{17}R)[1 + (1 - \kappa) {}^{15}R^\beta]}{{}^{15}R^\alpha(1 + {}^{31}R - {}^{17}R)} \quad (11)$$

165 For two reference materials, we can write two such equations and solve for two  
166 unknowns,  $\gamma$  and  $\kappa$ .  ${}^{15}R^\alpha$  and  ${}^{15}R^\beta$  represent *known* values for each reference material, and  ${}^{31}R$  is  
167 the observed quantity. Essentially, we are asking what values of  $\gamma$  and  $\kappa$  for a pair of known  ${}^{15}R^\alpha$   
168 and  ${}^{15}R^\beta$  values gives the observed  ${}^{31}R$  for each reference gas. Setting the two solutions for  $\gamma$   
169 equal allows us to determine  $\kappa$  and  $\gamma$  algebraically from the assigned  ${}^{15}R$  values of reference  
170 materials 1 and 2 ( ${}^{15}R_1^\alpha$ ,  ${}^{15}R_1^\beta$ ,  ${}^{15}R_2^\alpha$ ,  ${}^{15}R_2^\beta$ ), their observed  ${}^{31}R$  values ( ${}^{31}R_1$ ,  ${}^{31}R_2$ ), and the  ${}^{17}R$   
171 values ( ${}^{17}R_1$ ,  ${}^{17}R_2$ ):

$$\kappa = \frac{\frac{({}^{15}R_1^\alpha - {}^{31}R_1 + {}^{17}R_1)(1 + {}^{15}R_1^\beta)}{{}^{15}R_1^\alpha(1 + {}^{31}R_1 - {}^{17}R_1)} - \frac{({}^{15}R_2^\alpha - {}^{31}R_2 + {}^{17}R_2)(1 + {}^{15}R_2^\beta)}{{}^{15}R_2^\alpha(1 + {}^{31}R_2 - {}^{17}R_2)}}{\frac{{}^{15}R_2^\beta}{{}^{15}R_2^\alpha} - \frac{{}^{15}R_1^\beta}{{}^{15}R_1^\alpha}} \quad (12a)$$

$$\gamma = \frac{\frac{({}^{15}R_1^\alpha - {}^{31}R_1 + {}^{17}R_1)(1 + {}^{15}R_1^\beta)}{{}^{15}R_1^\alpha(1 + {}^{31}R_1 - {}^{17}R_1)} \left(\frac{{}^{15}R_2^\beta}{{}^{15}R_2^\alpha}\right) - \frac{({}^{15}R_2^\alpha - {}^{31}R_2 + {}^{17}R_2)(1 + {}^{15}R_2^\beta)}{{}^{15}R_2^\alpha(1 + {}^{31}R_2 - {}^{17}R_2)} \left(\frac{{}^{15}R_1^\beta}{{}^{15}R_1^\alpha}\right)}{\frac{{}^{15}R_2^\beta}{{}^{15}R_2^\alpha} - \frac{{}^{15}R_1^\beta}{{}^{15}R_1^\alpha}} \quad (12b)$$

172 After substituting  ${}^{45}R - {}^{15}R^\alpha - {}^{15}R^\beta$  for  ${}^{17}R$ , the equations for  $\gamma$  and  $\kappa$  can also be written as  
173 follows:

$$\kappa = \frac{\frac{({}^{45}R_1 - {}^{31}R_1 - {}^{15}R_1^\beta)(1 + {}^{15}R_1^\beta)}{{}^{15}R_1^\alpha(1 + {}^{15}R_1^\alpha + {}^{15}R_1^\beta + {}^{31}R_1 - {}^{45}R_1)} - \frac{({}^{45}R_2 - {}^{31}R_2 - {}^{15}R_2^\beta)(1 + {}^{15}R_2^\beta)}{{}^{15}R_2^\alpha(1 + {}^{15}R_2^\alpha + {}^{15}R_2^\beta + {}^{31}R_2 - {}^{45}R_2)}}{\frac{{}^{15}R_2^\beta}{{}^{15}R_2^\alpha} - \frac{{}^{15}R_1^\beta}{{}^{15}R_1^\alpha}} \quad (13a)$$

$$\gamma = \frac{\frac{({}^{45}R_1 - {}^{31}R_1 - {}^{15}R_1^\beta)(1 + {}^{15}R_1^\beta)}{{}^{15}R_1^\alpha(1 + {}^{15}R_1^\alpha + {}^{15}R_1^\beta + {}^{31}R_1 - {}^{45}R_1)} \left(\frac{{}^{15}R_2^\beta}{{}^{15}R_2^\alpha}\right) - \frac{({}^{45}R_2 - {}^{31}R_2 - {}^{15}R_2^\beta)(1 + {}^{15}R_2^\beta)}{{}^{15}R_2^\alpha(1 + {}^{15}R_2^\alpha + {}^{15}R_2^\beta + {}^{31}R_2 - {}^{45}R_2)} \left(\frac{{}^{15}R_1^\beta}{{}^{15}R_1^\alpha}\right)}{\frac{{}^{15}R_2^\beta}{{}^{15}R_2^\alpha} - \frac{{}^{15}R_1^\beta}{{}^{15}R_1^\alpha}} \quad (13b)$$

175 To obtain  ${}^{31}R_1$  and  ${}^{31}R_2$  in continuous-flow analysis, we measure two reference materials  
176 (CA08214 and 53504, Table 1) against a common working reference gas (wr), which is  
177 calibrated independently (“Lab 1 pure N<sub>2</sub>O direct injection” and “Lab 2 pure N<sub>2</sub>O direct  
178 injection” in Table 1). The working reference is a third calibrated reference material that  
179 normalizes different runs to the same reference frame:  
180

$${}^{31}R_1 = (1 + {}^{31}\delta_1){}^{31}R_{\text{wr}} \quad (14)$$

$${}^{31}R_2 = (1 + {}^{31}\delta_2){}^{31}R_{\text{wr}} \quad (15)$$

181 where  ${}^{31}R_1$  and  ${}^{31}R_2$  are calculated values that depend on  $\gamma$  and  $\kappa$ ,  ${}^{31}\delta$  is the measured ion  
 182 current ratio difference of sample (1 or 2) to working reference peak, and  ${}^{31}R_{\text{wr}}$  is an assumed  
 183 value calculated with constant  $\gamma$  and  $\kappa$  and assigned  ${}^{15}R^\alpha$ ,  ${}^{15}R^\beta$ , and  ${}^{17}R$ . Calculating  ${}^{31}R_{\text{wr}}$  with  
 184 constant  $\gamma$  and  $\kappa$  assumes that the working reference peak experiences a defined scrambling  
 185 behavior that could differ from that of a sample peak; ultimately, however,  ${}^{31}R_{\text{wr}}$  drops out of the  
 186 final  $\delta({}^{15}\text{N}^{\text{sp}})$  calculation, so this assumption has little effect.

187 The “algebraic” solution in pyisotopomer<sup>65</sup> uses  ${}^{31}R_1$  and  ${}^{31}R_2$  in eqns. (11) and (12) to  
 188 obtain  $\gamma$  and  $\kappa$ . The “least\_squares” method in pyisotopomer<sup>65</sup> solves eqns. (14) and (15) for  $\gamma$   
 189 and  $\kappa$  iteratively with a least squares optimization routine. We present a full discussion of the  
 190 appropriate use of the algebraic and least squares methods in section 4.2.

191 Some of the isotopomer literature obtains  ${}^{15}R^{\text{bulk}}$  and  ${}^{15}R^\alpha$  by regression between true and  
 192 measured values of reference materials, inferring  ${}^{15}R^\beta$  indirectly<sup>20</sup>. In this case, a linear  
 193 calibration curve replaces the scrambling correction. However, a linear calibration curve just  
 194 based on “known”  $\delta({}^{15}\text{N}^\alpha)$  values will fail unless the “known”  $\delta({}^{15}\text{N}^{\text{sp}})$  values are constant — in  
 195 other words, a linear calibration curve is only acceptable if the unknowns are close in their  
 196  $\delta({}^{15}\text{N}^{\text{sp}})$  to those of the reference material. It is not accurate if unknowns diverge in their  $\delta({}^{15}\text{N}^{\text{sp}})$   
 197 from that of the reference material(s). This is because the measured  ${}^{31}\delta$  value depends on both  
 198  ${}^{15}R^\alpha$  and  ${}^{15}R^\beta$  (Supplementary text S2).

199 To obtain  ${}^{15}R^\alpha$ ,  ${}^{15}R^\beta$ , and  ${}^{18}R$  of unknowns, pyisotopomer solves for these values from  
 200 eqns. (3), (4), (5), and (10), using  ${}^{31}R$ ,  ${}^{45}R$ ,  ${}^{46}R$ ,  $\gamma$ , and  $\kappa$  as input terms<sup>50</sup>. The delta values  $\delta({}^{15}\text{N}^\alpha)$ ,  
 201  $\delta({}^{15}\text{N}^\beta)$ ,  $\delta({}^{15}\text{N}^{\text{sp}})$ ,  $\delta({}^{15}\text{N}^{\text{bulk}})$ , and  $\delta({}^{18}\text{O})$  are calculated from  ${}^{15}R^\alpha$ ,  ${}^{15}R^\beta$ , and  ${}^{18}R$  relative to primary  
 202 reference scales ( ${}^{15}R$  from atmospheric  $\text{N}_2$ ,  ${}^{17}R$  and  ${}^{18}R$  from VSMOW; if desired, the values of  
 203 primary reference scale ratios may be adjusted with keyword arguments, as described in the  
 204 pyisotopomer Documentation<sup>65</sup>). Additionally, if  $\Delta^{17}\text{O}$  has been measured separately<sup>60,62,63</sup>,  
 205 pyisotopomer can take this value into account in the calculation of  $\delta({}^{15}\text{N}^\alpha)$ ,  $\delta({}^{15}\text{N}^\beta)$ ,  $\delta({}^{15}\text{N}^{\text{sp}})$ ,  
 206  $\delta({}^{15}\text{N}^{\text{bulk}})$ , and  $\delta({}^{18}\text{O})$ .

207

### 208 3. Experimental methods

#### 209 3.1 Preparation and analysis of dissolved $\text{N}_2\text{O}$ reference materials

210 A series of dissolved  $\text{N}_2\text{O}$  reference materials (Table 1) were prepared and analyzed in  
 211 both Lab 1 and Lab 2. Reference materials were prepared by filling 160-mL glass serum bottles  
 212 (Wheaton) with de-ionized water and removing a 4-mL headspace (Lab 1) or 10 to 20-mL  
 213 headspace (Lab 2), then capped with a gray butyl rubber septum (National Scientific) and sealed  
 214 with an aluminum crimp seal. These bottles were purged with helium for 90 minutes at yields a  
 215 minimum flow rate of 100 mL/min to remove all background  $\text{N}_2\text{O}$ . The purged bottles were then  
 216 injected with 2 to 43 nmol  $\text{N}_2\text{O}$  to give  $\text{N}_2\text{O}$  concentrations of 13 to 275 nM (Lab 1) or 1 to 60  
 217 nmol  $\text{N}_2\text{O}$  to give  $\text{N}_2\text{O}$  concentrations of 6 to 427 nM (Lab 2) in a matrix of He or synthetic air  
 218 (Table 1) using a gas-tight syringe. Reference materials prepared in Lab 1 were preserved with  
 219 100  $\mu\text{L}$  saturated mercuric chloride ( $\text{HgCl}_2$ ) solution; those prepared in Lab 2 contained no  
 220 added preservative. For Lab 1, atmosphere-equilibrated seawater was prepared by filtering  
 221 surface seawater (collected in Half Moon Bay, CA) through a 0.22 mm Sterivex filter, allowing  
 222 it to undergo static equilibration with outdoor air for three days, then re-filtering into 160-mL  
 223 serum bottles, removing a 1-mL headspace, and preserving with 100  $\mu\text{L}$  saturated mercuric

224 chloride solution. For Lab 2, atmosphere-equilibrated reference materials were prepared by  
225 purging either de-ionized water or a sodium chloride solution with helium, allowing it to undergo  
226 static equilibration with outdoor air for three days, filling into 160-mL serum bottles, and  
227 removing a 10-mL headspace. While we were able to correct for these differences in reference  
228 material preparation, future intercalibration efforts should aim to prepare reference materials the  
229 same way in participating laboratories. In addition, the linearity relationships should be  
230 determined from analyzing different amounts of gaseous reference materials, to separate any  
231 artifacts due to preparation and extraction of dissolved N<sub>2</sub>O reference materials from the  
232 abundance linearity of the isotope ratio mass spectrometer itself.

233 Reference materials were run in the same format as samples to account for any potential  
234 fractionation associated with the purge-and-trap system. The magnitude of such fractionation  
235 was quantified for Lab 1 by running aliquots of the pure N<sub>2</sub>O reference tank in sample format;  
236 this test yielded offsets of (0.22±0.52) ‰ for  $\delta(^{15}\text{N}^{\text{bulk}})$  and (0.16±0.62) ‰ for  $\delta(^{18}\text{O})$  vs. the  
237 reference tank injection (see Supplementary text S3 for a full discussion of potential  
238 fractionation effects in the purge-and-trap system).

239 The reference gases were calibrated independently by J. Mohn (EMPA; mini-QCLAS  
240 aerodyne) or S. Toyoda (Tokyo Tech; IRMS), except for one internal standard used by Lab 1  
241 (B6; Table 1). The  $\delta(^{17}\text{O})$  values for each gas were calculated assuming a mass-dependent  
242 relationship between  $^{17}\text{R}$  and  $^{18}\text{R}$  (eqn. 5).

243 Reference gases and samples were measured on Thermo Finnigan DELTA V Plus isotope  
244 ratio mass spectrometers (IRMS; Thermo Fisher Scientific, Waltham, MA) in Labs 1 and 2. Each  
245 IRMS had Faraday cups configured to simultaneously measure  $m/z$  30, 31, 44, 45, and 46. The  
246 measurements from the Lab 1 DELTA V Plus were made under normal operating conditions,  
247 using an ionization energy of 124 eV, accelerating voltage of 3 kV, emission current of 1.50 mA,  
248 and box and trap currents of 0.68 and 0.82 mA, respectively. The measurements from the Lab 2  
249 DELTA V Plus were made under normal operating conditions, using an ionization energy of 110  
250 eV, accelerating voltage of 3 kV, emission current of 1.00 mA, and box and trap currents of 0.45  
251 and 0.55 mA, respectively. Reference materials and samples were analyzed on custom purge-  
252 and-trap systems coupled to each IRMS, which was run in continuous flow mode<sup>66</sup> (Table 1).  
253 The two systems had slight differences in the purge-and-trap method: in Lab 1, liquid from each  
254 sample bottle was transferred under helium pressure to a sparging column to extract the  
255 dissolved gases<sup>67</sup>; in Lab 2, each sample was extracted by purging directly from the bottle. The  
256 effects of these differences are discussed further in Results and Discussion.

257

## 258 **3.2 Data corrections**

### 259 **3.2.1 Linearity relation**

260 The measured ion current ratios 31/30, 45/44, and 46/44 of each sample peak were  
261 divided by those of the working reference peak. This produced three molecular isotope delta  
262 values  $^{31}\delta+1$ ,  $^{45}\delta+1$ , and  $^{46}\delta+1$ , where  $\delta = R_s/R_{wr} - 1$ , with the subscripts “s” and “wr” denoting  
263 sample and working reference, respectively (Figure 1, Step 5).

264 The  $\delta$  values were corrected for the effect of peak size<sup>33</sup>. For Lab 1, this was  
265 accomplished by running six reference materials (reference gases S2, B6, A01, CA06261, 90454,  
266 and 94321; Table 1) in size series ranging from 2-43 nmol N<sub>2</sub>O. For Lab 2, three reference  
267 materials (CA06261, 53504, and CA08214) were run in size series ranging from 1-60 nmol N<sub>2</sub>O  
268 (Figure 1, Step 6).



269 To obtain a single size correction slope from multiple size series, we used the dummy-  
 270 variable method of combining regressions<sup>68</sup>. The dummy variable method is an improvement  
 271 over simply averaging each individually calculated slope because it implicitly weighs each size  
 272 series by its informativeness, producing a slope that is more likely to reflect the overall linearity  
 273 behavior of the instrument<sup>68</sup>. For a given material, each measured  $\delta+1$  is a linear function of its  
 274 peak area ( $A$ ) plus an intercept ( $\gamma_1 + \gamma_2 D_2 + \gamma_3 D_3$ ):

$$\delta + 1 = \hat{\beta}A + \gamma_1 + \gamma_2 D_2 + \gamma_3 D_3 \quad (16)$$

275 where  $\hat{\beta}$  represents the regression coefficient for a particular peak area (for  $m/z$  31,45, or 46),  
 276 obtained by multiple linear regression. The intercept for reference material 1 is  $\gamma_1$ .  $D_2$  and  $D_3$  are  
 277 ‘dummy variables’ to adjust  $\gamma_1$  by an appropriate intercept for reference material 2 ( $\gamma_1 + \gamma_2$ ) and  
 278 reference material 3 ( $\gamma_1 + \gamma_3$ ). Thus, for reference material 1,  $D_2 = D_3 = 0$ ; for reference material  
 279 2,  $D_2 = 1$  and  $D_3 = 0$ ; for reference material 3,  $D_2 = 0$  and  $D_3 = 1$ . These dummy variables allow  
 280 us to obtain one slope for each isotope delta from multiple datasets accounting for differences in  
 281 intercept, with each reference material weighted by its spread in the  $x$ -axis range. Thus, slopes  
 282  $\hat{\beta}_{31}$ ,  $\hat{\beta}_{45}$ , and  $\hat{\beta}_{46}$  were calculated for  $^{31}\delta+1$ ,  $^{45}\delta+1$ , and  $^{46}\delta+1$ , respectively, each using eqn. (16).

283 To normalize measured values of  $\delta+1$  to a common peak area, we first calculated the  
 284  $(\delta+1)_0$  that would be measured at  $m/z$  44 peak area  $A_0$ :

$$(\delta + 1)_0 = \hat{\beta}(A_0) + \gamma_1 + \gamma_2 D_2 + \gamma_3 D_3 \quad (17)$$

285 Note that  $(\delta+1)_0$  is still a function of  $\hat{\beta}$ , the intercepts  $\gamma_1$ ,  $\gamma_2$ ,  $\gamma_3$ , and the dummy variables  $D_2$  and  
 286  $D_3$ . To obtain the difference  $\delta_0 - \delta$  from the measured  $m/z$  44 peak area  $A$ , we subtract eqn. (17)  
 287 from eqn. (16), to obtain:

$$(\delta + 1)_0 - (\delta + 1) = \hat{\beta}(A_0 - A)$$

288 In this case, the size-corrected molecular isotope ratio,  $\delta_0$ , for each sample with measured  $\delta$  and  
 289 peak area  $A$  is given by:

$$(\delta + 1)_0 = \hat{\beta}(A_0 - A) + (\delta + 1) \quad (18)$$

290 Eqn. (18) is simply a function of the slope  $\hat{\beta}$ , the measured ( $A$ ) and target ( $A_0$ )  $m/z$  44 peak areas,  
 291 and the measured  $\delta$ . Thus, eqn. (18) can be applied across a range of peak areas and  $\delta$  values to  
 292 normalize these  $\delta$  values to a common peak area. Using this method, we normalized the  
 293 measured  $^{31}\delta+1$ ,  $^{45}\delta+1$ , and  $^{46}\delta+1$  of each sample to a peak area ( $A_0$ ) of 20 Vs (volt seconds),  
 294 equivalent to 10 nmol  $N_2O$  on the Lab 1 IRMS (Figure 1, Step 7). We note that the linearity  
 295 correction estimated here implicitly assumes that samples and reference materials are affected by  
 296 the same relative blank size.

297

### 298 3.2.2 Scale normalization and calculation of $^{17}R$

299 After applying the linearity correction, a scale normalization was applied to  $^{45}\delta$  and  $^{46}\delta$   
 300 (Figure 1, Step 8). The scale normalization for  $^{45}\delta$  and  $^{46}\delta$  needs to be carried out before the  
 301 scrambling correction (which is essentially a scale normalization of  $^{31}\delta$ ); otherwise, the wrong  
 302 bulk  $^{15}N/^{14}N$  and  $^{18}O/^{16}O$  ratios are implied. Furthermore, while the  $\gamma$  and  $\kappa$  calculations  
 303 constrain the differences between  $\delta(^{15}N^a)$  and  $\delta(^{15}N^b)$ , their absolute values are governed by  
 304  $\delta(^{15}N^{bulk})$ , necessitating that the “correct”, normalized value of  $^{45}\delta$  be input to the scrambling  
 305 equations. This scale normalization is a replacement for any scale normalization or offset  
 306 correction to the final output  $\delta$  values, such as the one-point and two-point offset corrections  
 307 calculated and applied in Mohn et al. (2014).

308 A scale normalization was calculated for each run included in the intercalibration  
 309 exercise. Since assigned values of  $^{45}R$  and  $^{46}R$  for each reference gas were unavailable, assigned

310  $^{45}R$  and  $^{46}R$  were calculated from assigned  $^{15}R^\alpha$ ,  $^{15}R^\beta$ , and  $^{18}R$  and eqns. (3), (4), and (5) (Table  
 311 1), assuming  $^{17}R_{VSMOW} = 0.0003799^{69}$  and  $^{18}R_{VSMOW} = 0.0020052^{58}$ . Next, the assigned  $^{45}R$  and  
 312  $^{46}R$  for each reference gas were divided by the known  $^{45}R$  and  $^{46}R$  of the direct N<sub>2</sub>O reference  
 313 injection to obtain assigned  $^{45}\delta$  and  $^{46}\delta$  for each reference material. Then, these assigned  $^{45}\delta$  and  
 314  $^{46}\delta$  values were compared to measured  $^{45}\delta$  and  $^{46}\delta$  values, and scale normalization coefficients  
 315 were calculated following the logarithmic scale normalization outlined in Kaiser et al. (2007):

$$\ln(1 + ^{45}\delta^n) = m \ln(1 + ^{45}\delta) + b$$

317 where  $^{45}\delta^n$  is the normalized  $^{45}\delta$ , “m” is the slope of the regression of  $\ln(1+^{45}\delta^n)$  vs.  
 318  $\ln(1+^{45}\delta)$ , and “b” is the intercept (and likewise for  $^{46}\delta$ ). From this regression, the normalized  $\delta$   
 319 values can be obtained:

$$1 + ^{45}\delta^n = e^b (1 + ^{45}\delta)^m \quad (19)$$

320 For the working reference, the values of  $^{45}\delta$  and  $^{45}\delta^n$  are equal to zero, so the intercept  $b$   
 321 should be equal to or very close to zero. The benefit of the logarithmic normalization is that,  
 322 unlike a linear scale normalization, it is scale-invariant<sup>62</sup>: essentially, the logarithmic scale  
 323 normalization does not skew the data towards extremely high or low values, and instead equally  
 324 weights all data points<sup>62</sup>.

325 Next, a measured  $^{18}R$  was derived from the scale-normalized  $^{45}R$  and  $^{46}R$  for each sample  
 326 and reference material (Figure 1, Step 8). The size correction and scale normalization were  
 327 carried out in the pyisotopomer spreadsheet template; the  $^{18}R$  derivation from the scale-  
 328 normalized  $^{45}R$  and  $^{46}R$  was the first step accomplished by the pyisotopomer code<sup>65</sup>. Deriving  $^{18}R$   
 329 was accomplished by assuming a mass-dependent relationship between  $^{17}R$  and  $^{18}R$  (eqn. 5) and  
 330  $^{15}R^\alpha = ^{15}R^\beta = ^{15}R^{bulk}$ . These terms are then substituted into eqns. (3) and (4) to yield:

$$^{45}R = 2^{15}R^{bulk} + ^{17}R_{VSMOW} \left( \frac{^{18}R}{^{18}R_{VSMOW}} \right)^\beta (\Delta^{17}O + 1) \quad (20)$$

$$^{46}R = ^{18}R + 2^{15}R^{bulk} \left[ ^{17}R_{VSMOW} \left( \frac{^{18}R}{^{18}R_{VSMOW}} \right)^\beta (\Delta^{17}O + 1) \right] + (^{15}R^{bulk})^2 \quad (21)$$

331 Note that the slope  $\beta$  of the mass-dependent relationship between  $^{17}R$  and  $^{18}R$  is an  
 332 adjustable parameter in the code (default: 0.516), and  $\Delta^{17}O$  for each reference material may be  
 333 entered in the data correction template and subsequently accounted for in this correction (default:  
 334 0 ‰). Eqns. (20) and (21) were then solved for  $^{18}R$  and  $^{15}R^{bulk}$  to obtain an estimated  $^{18}R$  and  
 335  $^{15}R^{bulk}$  for each sample and reference material, and  $^{17}R$  was calculated from  $^{18}R$  according to eqn.  
 336 (5). The resulting  $^{18}R$ ,  $^{17}R$ , and  $^{15}R^{bulk}$  were used in the scrambling calculation. They contain an  
 337 error due to the assumption that  $^{15}R^\alpha = ^{15}R^\beta = ^{15}R^{bulk}$ , although the magnitude of this error should  
 338 be small<sup>62</sup>. Later, the isotopomer calculation solves for  $^{15}R^\alpha$  and  $^{15}R^\beta$  separately and thus corrects  
 339 this error.

340 In the intercalibration exercise, values of  $m$  and  $b$  were calculated from the slopes of  
 341 assigned  $^{45}\delta^a$  vs. measured  $^{45}\delta$  and assigned  $^{46}\delta^a$  vs. measured  $^{46}\delta$  from the reference materials in  
 342 each run. These runs took place in February 2021 for Lab 1 and August 2020 and November  
 343 2020 for Lab 2. Combined, the scale normalization and size correction should account for any  
 344 size- or isotope-ratio dependent effects, including those of a blank, linearity, or fractionation in  
 345 the GasBench.

### 346 3.2.3 Calculating $^{31}R_m$ of the direct N<sub>2</sub>O reference injection

348 We used the same scrambling coefficients for the working reference gas as for the  
349 samples. We recommend that the user calculates the  $^{31}R$  of the direct reference injection ( $^{31}R_{wr}$  in  
350 eqns. 14 and 15) with the following sequence of steps: 1) calculate  $^{31}R_{wr}$  from eqn. (10) with  
351 either  $\gamma = \kappa = 0.1$ , which reflects commonly reported values<sup>36,50,54</sup>, or an *a priori* estimate, if  
352 available (Figure 1, Step 9); 2) use that  $^{31}R_{wr}$  to correct data from two reference materials and  
353 from those reference materials, obtain  $\gamma$  and  $\kappa$  from eqns. (11) and (12) (Figure 1, Step 10); 3)  
354 use these updated  $\gamma$  and  $\kappa$  to re-calculate  $^{31}R_{wr}$  from eqn. (10) (Figure 1, Step 11). The input  $\gamma$  and  
355  $\kappa$  (used to calculate  $^{31}R_{wr}$ ) and output  $\gamma$  and  $\kappa$  (calculated from paired reference materials) should  
356 converge quickly, so one iteration of this process should be sufficient. This value of  $^{31}R_{wr}$  can  
357 then be used to convert  $^{31}\delta$  to  $^{31}R_s$ . The user should also note that there are likely to be multiple  
358 pairings of input and output  $\gamma$  and  $\kappa$  that will consistently yield indistinguishable delta values.  
359

### 360 3.2.4 IRMS scrambling calibration and isotopomer calculation

361 The "Scrambling" function of pyisotopomer was used to calculate  $\gamma$  and  $\kappa$  algebraically  
362 from all possible pairings of reference materials CA08214 and 53504 measured on a given IRMS  
363 (Lab 1 or Lab 2; Figure 1, Step 13). The reference materials CA08214 and 53504 were chosen  
364 because of their 113 ‰  $\delta(^{15}N^{sp})$  difference (see Results and Discussion for a description of how  
365 to choose reference material pairings), as well as the range of  $\delta(^{15}N^{\alpha})$ ,  $\delta(^{15}N^{\beta})$ ,  $\delta(^{15}N^{bulk})$ , and  
366  $\delta(^{18}O)$  spanned by the two reference materials, which represent values found typically in  
367 culture<sup>52,70</sup> and nature<sup>26,31</sup>. One-week running averages of  $\gamma$  and  $\kappa$  were calculated to smooth their  
368 variation and used to obtain position-dependent  $\delta$  values for unknowns and reference materials  
369 run as unknowns for quality control (CA06261, S2, B6, and atmosphere-equilibrated seawater),  
370 using the "Isotopomers" function of pyisotopomer (Figure 1, Step 14).

371 For comparison, this exercise was repeated, calculating  $\gamma$  and  $\kappa$  iteratively with the least  
372 squares optimization (Figure 1, Step 12). The mean algebraic  $\gamma$  and  $\kappa$  from the paired reference  
373 materials CA08214 and 53504 was used as the initial guess for the least squares solver. In this  
374 case, reference materials CA08214 and CA06261 were used to calculate the least squares  $\gamma$  and  
375  $\kappa$ , because these reference materials are close in their calibrated isotopomer values to natural  
376 abundance unknowns. As above,  $\gamma$  and  $\kappa$  were combined into a one-week running average; these  
377 running averages of  $\gamma$  and  $\kappa$  for each system were used to obtain position-dependent  $\delta$  values for  
378 reference materials and unknowns in the intercalibration exercise (Figure 1, Step 14). The  
379 analytical precisions of  $\delta(^{15}N^{\alpha})$ ,  $\delta(^{15}N^{\beta})$ ,  $\delta(^{15}N^{sp})$ ,  $\delta(^{15}N^{bulk})$ , and  $\delta(^{18}O)$  produced by each method  
380 are presented in the Results and Discussion.

381  $N_2O$  amounts were obtained from the  $m/z$  44 peak area and instrument  $N_2O$  sensitivity<sup>67</sup>.  
382 To obtain the conversion factor between peak area and amount of  $N_2O$ , the peak areas for  
383 reference material amounts from 1 to 40 nmol  $N_2O$  were recorded. Standard deviations for  
384 inferred  $N_2O$  amounts of replicate unknown samples were 0.07 nmol for Lab 1, and 0.19 nmol  
385 for Lab 2. All data corrections are described in the README documents associated with  
386 pyisotopomer on the Python Package Index<sup>65</sup>.  
387

### 388 3.3 Lake water unknowns

389 To validate the scrambling calibration, samples of unknown isotopic composition were  
390 collected from Lake Lugano, Switzerland in July 2020 and analyzed separately by both Lab 1  
391 and Lab 2. The samples were collected at depths of 10 and 90 meters, including six replicate  
392 bottles at each depth. Samples were collected into 160-mL glass serum bottles (Wheaton),  
393 overflowing each bottle twice, closing bubble-free, and removing liquid to form a 10-mL

394 headspace comprised of air. Based on the northern hemisphere monthly mean tropospheric N<sub>2</sub>O  
395 mole fraction when the samples were collected in July, 2020<sup>71</sup>, an atmospheric headspace of this  
396 volume would have contained 0.13 nmol N<sub>2</sub>O. For Lab 2, where the full amount of N<sub>2</sub>O in the  
397 sample is measured, incorporation of the headspace into the measurement results in a 0.13 nmol  
398 overestimation of the amount of N<sub>2</sub>O in the sample<sup>71</sup>. For Lab 1, where 2 mL sample liquid is  
399 left behind post-analysis, equilibration the 10-mL headspace during sample storage results in  
400 either an underestimate (0.12 nmol) or overestimate (0.10 nmol) of N<sub>2</sub>O in the sample,  
401 depending on its concentration. In both cases, these errors are similar to the analytical precision  
402 of the N<sub>2</sub>O amount measurement. Each sample was capped with a gray butyl septum (National  
403 Scientific) and sealed with an aluminum crimp seal. Samples were promptly preserved with 100  
404  $\mu$ L saturated mercuric chloride solution and stored at lab temperature (20-22°C). The isotope  
405 fractionation associated with N<sub>2</sub>O partitioning, defined as the isotope ratio of the gas phase  
406 divided by the isotope ratio of the liquid phase, (<sup>15</sup> $\epsilon$  = -0.7 ‰, <sup>18</sup> $\epsilon$  = -1.1 ‰, 298.2 K) falls  
407 within the analytical uncertainty<sup>72</sup>. The six replicate bottles at each depth were split into two  
408 groups of three replicate bottles to be measured by Lab 1 and Lab 2, respectively.  
409

## 410 **4. Results and Discussion**

### 411 **4.1 Linearity relation**

412 Linearity relations were calculated using the dummy variable method described in  
413 Section 3.2.1 and applied to the intercalibration data as follows. A linearity relation was  
414 determined for Lab 1 in February 2021 (Figure 2a-c) and applied to lake water samples run in  
415 Lab 1 and reference materials prepared and run in Lab 1. Reference materials prepared in Lab 2  
416 but run in Lab 1 exhibited statistically distinct linearity slopes from those both prepared and run  
417 in Lab 1; thus, a separate linearity relation was applied to these reference materials (but not to the  
418 lake water samples) (Figure 2d-f). A linearity relation was determined for Lab 2 in May 2020  
419 (Figure 2g-i) and applied to lake water samples and reference materials run in Lab 2. As  
420 previously observed<sup>73</sup>, for each linearity relation, the slopes of the fits for individual reference  
421 materials were identical within error. The linearity correction reduced the spread of measured  
422 molecular isotope ratios across size series of each given reference material (Figure S2).  
423  
424

### 425 **4.2 IRMS scrambling calibration**

426 For both labs, the “algebraic” solution produced reasonable values of  $\gamma$  and  $\kappa$  (i.e.,  
427 between 0 and 1) for reference material pairings involving the reference material 53504 ( $\delta(^{15}\text{N}^{\text{sp}})$   
428 = -93 ‰). The mean  $\gamma$  and  $\kappa$  calculated for Lab 1 from reference materials 53504 and CA08214  
429 were 0.174±0.022 and 0.083±0.022, respectively (Table S2). In August 2020, the mean  $\gamma$  and  $\kappa$   
430 calculated for Lab 2 from the same two reference materials were 0.095±0.011 and 0.091±0.010,  
431 respectively (Table S2). In November 2020,  $\gamma$  and  $\kappa$  for Lab 2 were slightly different but within  
432 1 $\sigma$  of the values measured in August 2020 (0.091±0.013 and 0.086±0.013, respectively; Table  
433 S2). Other reference materials paired with 53504 produced similar values of  $\gamma$  and  $\kappa$ . The  
434 difference  $\gamma - \kappa$  was also consistent for reference material pairings with 53504: for Lab 1,  $\gamma - \kappa$   
435 was 0.090-0.091, and for Lab 2, it was 0.003-0.005 (Table S2).

436 For pairings with 53504, the  $\delta(^{15}\text{N}^{\text{sp}})$  difference between both reference materials was  
437 greater than 100 ‰. Pairs of reference materials with smaller  $\delta(^{15}\text{N}^{\text{sp}})$  differences produced more  
438 variable  $\gamma$  and  $\kappa$  values with the algebraic solution, which sometimes fell outside the physically  
439 plausible range between 0 and 1. For example, in Lab 1, the pairing of CA06261 and CA08214

440 produced  $\gamma$  and  $\kappa$  values of  $0.01 \pm 0.23$  and  $-0.08 \pm 0.23$ , respectively. In this case, the  
 441 measurement uncertainty was too large — and the  $\delta(^{15}\text{N}^{\text{sp}})$  values too close — for the scrambling  
 442 coefficients to be adequately determined. What matters, however, is that the difference between  $\gamma$   
 443 and  $\kappa$  is accurate; as the results show, the absolute values are less important (and can even be  
 444 negative, greater than 1, or otherwise “unphysical”).

445 To understand the uncertainty in  $\gamma$  and  $\kappa$  calculated from equations 11 and 12, we define a  
 446 variable  $d$ , which allows us to express the analytical solution for  $\gamma$  and  $\kappa$  (eqns. 13a and 13b) in  
 447 terms of  $\delta(^{15}\text{N}^{\text{sp}})$ ,  $\delta(^{15}\text{N}^{\text{sp}})$ , and  $\delta(^{15}\text{N}^{\text{sp}})$ :

$$d = \frac{(^{15}\text{R}^{\beta} + ^{31}\text{R} - ^{45}\text{R})(1 + ^{15}\text{R}^{\beta})}{^{15}\text{R}_{\text{atm}}(1 + ^{15}\text{R}^{\alpha} + ^{15}\text{R}^{\beta} + ^{31}\text{R} - ^{45}\text{R})} \quad (22)$$

448  
 449 The value of  $d$  is similar for all samples and reference gases run on a given IRMS and  
 450 depends primarily on the difference  $^{31}\text{R} - ^{45}\text{R}$ . Using  $\delta$  notation, i.e.,  $\delta(^{15}\text{N}) = ^{15}\text{R}/^{15}\text{R}_{\text{atm}} - 1$ , and  
 451 dropping the label “ $^{15}\text{N}$ ” for brevity, eqns. (13a) and (13b) can be written as follows:

$$\kappa = \frac{\frac{d_2}{1 + \delta_2^{\alpha}} - \frac{d_1}{1 + \delta_1^{\alpha}}}{\frac{1 + \delta_2^{\beta}}{1 + \delta_2^{\alpha}} - \frac{1 + \delta_1^{\beta}}{1 + \delta_1^{\alpha}}} = \frac{\frac{d_2}{1 + \delta_2^{\alpha}} - \frac{d_1}{1 + \delta_1^{\alpha}}}{\frac{\delta_1^{\text{sp}}}{1 + \delta_1^{\alpha}} - \frac{\delta_2^{\text{sp}}}{1 + \delta_2^{\alpha}}} \quad (23a)$$

$$\begin{aligned} \gamma &= \frac{\frac{d_2}{1 + \delta_2^{\alpha}} \left( \frac{1 + \delta_1^{\beta}}{1 + \delta_1^{\alpha}} \right) - \frac{d_1}{1 + \delta_1^{\alpha}} \left( \frac{1 + \delta_2^{\beta}}{1 + \delta_2^{\alpha}} \right)}{\frac{1 + \delta_2^{\beta}}{1 + \delta_2^{\alpha}} - \frac{1 + \delta_1^{\beta}}{1 + \delta_1^{\alpha}}} \\ &= \frac{\frac{d_2}{1 + \delta_2^{\alpha}} \left( \frac{1 + \delta_1^{\beta}}{1 + \delta_1^{\alpha}} \right) - \frac{d_1}{1 + \delta_1^{\alpha}} \left( \frac{1 + \delta_2^{\beta}}{1 + \delta_2^{\alpha}} \right)}{\frac{\delta_1^{\text{sp}}}{1 + \delta_1^{\alpha}} - \frac{\delta_2^{\text{sp}}}{1 + \delta_2^{\alpha}}} \end{aligned} \quad (23b)$$

452 The denominators of these expressions can be approximated by the difference  $\delta_1^{\text{sp}} - \delta_2^{\text{sp}}$ .  
 453 Thus, if the site preferences of the reference gases are similar, the value of the denominator  
 454 approaches zero and the solutions will become uncertain due to the finite measurement error.  
 455 Then, the question arises, how far apart must the site preferences of the reference materials be to  
 456 obtain robust solutions?

457 The general form of uncertainty propagation in a variable  $a$  with respect to the  
 458 observations ( $y_i$ ) is given by the following equation<sup>74</sup>:

$$459 \quad \sigma_a^2 = \sum_i \sigma_i^2 \left( \frac{\partial a}{\partial y_i} \right)^2$$

460 where  $\sigma_a$  is the uncertainty in  $a$ ,  $y_i$  is an individual observation, and  $\sigma_i$  is the uncertainty in the  
 461 observation  $y_i$ . Ignoring the uncertainties in  $^{45}\text{R}$  and the assigned position-dependent  $^{15}\text{R}$  values,  
 462 the uncertainty in  $\kappa$  can be calculated as:

$$463 \quad \sigma_{\kappa}^2 = \sigma_{^{31}\text{R}_1}^2 \left( \frac{\partial \kappa}{\partial ^{31}\text{R}_1} \right)^2 + \sigma_{^{31}\text{R}_2}^2 \left( \frac{\partial \kappa}{\partial ^{31}\text{R}_2} \right)^2$$

464

$$465 \quad \frac{\partial \kappa}{\partial^{31}R_1} = \frac{\frac{-(1 + {}^{15}R_1^\alpha)(1 + {}^{15}R_1^\beta)}{{}^{15}R_1^\alpha(1 + {}^{15}R_1^\alpha + R_1^\beta + {}^{31}R_1 - {}^{45}R_1)^2}}{\frac{\delta_1^{\text{sp}}}{1 + \delta_1^\alpha} - \frac{\delta_2^{\text{sp}}}{1 + \delta_2^\alpha}} \approx \frac{-1}{{}^{15}R_1^\alpha(\delta_1^{\text{sp}} - \delta_2^{\text{sp}})}$$

466

$$\frac{\partial \kappa}{\partial^{31}R_2} = \frac{\frac{-(1 + {}^{15}R_2^\alpha)(1 + {}^{15}R_2^\beta)}{{}^{15}R_2^\alpha(1 + {}^{15}R_2^\alpha + R_2^\beta + {}^{31}R_2 - {}^{45}R_2)^2}}{\frac{\delta_1^{\text{sp}}}{1 + \delta_1^\alpha} - \frac{\delta_2^{\text{sp}}}{1 + \delta_2^\alpha}} \approx \frac{-1}{{}^{15}R_2^\alpha(\delta_1^{\text{sp}} - \delta_2^{\text{sp}})}$$

467

468 Assuming  $\sigma_{31R}/{}^{15}R^\alpha = \sigma_{31R_1}/{}^{15}R_1^\alpha = \sigma_{31R_2}/{}^{15}R_2^\alpha$ , then

$$469 \quad \sigma_\kappa^2 \approx 2 \left( \frac{\sigma_{31R}}{{}^{15}R^\alpha} \right)^2 \left( \frac{1}{\delta_1^{\text{sp}} - \delta_2^{\text{sp}}} \right)^2$$

470 or

$$\sigma_\kappa \approx \sqrt{2} \frac{\sigma({}^{31}R)}{{}^{15}R^\alpha} \frac{1}{|\delta_1^{\text{sp}} - \delta_2^{\text{sp}}|} \quad (24a)$$

471 Similarly, for  $\gamma$ :

$$\sigma_\gamma \approx \sqrt{2} \frac{\sigma({}^{31}R)}{{}^{15}R^\beta} \frac{1}{|\delta_1^{\text{sp}} - \delta_2^{\text{sp}}|} \quad (24b)$$

472 where  $\sigma({}^{31}R)/{}^{15}R$  can be approximated by the measurement uncertainty in  ${}^{31}\delta$  and  
 473  $|\delta_1^{\text{sp}} - \delta_2^{\text{sp}}|$  is the absolute value of the difference in assigned site preferences between the two  
 474 reference materials. This means that for a measurement uncertainty in  ${}^{31}\delta$  of 1 ‰ and a  $\delta({}^{15}\text{N}^{\text{sp}})$   
 475 difference of 10 ‰ between the two reference materials,  $\gamma$  and  $\kappa$  would have absolute  
 476 uncertainties of 0.14. This uncertainty translates into a relative uncertainty of about 30 % for the  
 477  $\delta({}^{15}\text{N}^{\text{sp}})$  value of an unknown sample – far too high for practical applications (Supplementary  
 478 text S4). A  $\delta({}^{15}\text{N}^{\text{sp}})$  difference of 100 ‰ would give a more useful absolute uncertainty of 0.014  
 479 for  $\gamma$  and  $\kappa$ .

480 These theoretical uncertainties are reflected in the experimental data. For Lab 1, the  
 481 reference materials 53504 ( $\delta({}^{15}\text{N}^{\text{sp}}) = -92.73$  ‰) and CA08214 ( $\delta({}^{15}\text{N}^{\text{sp}}) = 20.54$  ‰) yielded  $\gamma =$   
 482  $0.174 \pm 0.022$  and  $\kappa = 0.083 \pm 0.022$ . The standard deviation of  ${}^{31}\delta$  was 1.89 ‰ ( $n = 12$ ). This  
 483 produces an estimated uncertainty in  $\gamma$  and  $\kappa$  of  $\sqrt{2}(1.89 \text{ ‰})/(113.27 \text{ ‰}) = 0.024$ , which agrees  
 484 well with the experimental data. Similarly, reference materials 53504 and CA06261 ( $\delta({}^{15}\text{N}^{\text{sp}}) =$   
 485  $27.07$  ‰) yielded  $\gamma = 0.163 \pm 0.018$  and  $\kappa = 0.073 \pm 0.018$ . The standard deviation of  ${}^{31}\delta$  was 1.58  
 486 ‰ ( $n = 10$ ), and the  $\delta({}^{15}\text{N}^{\text{sp}})$  difference was 119.80 ‰. This produced an estimated uncertainty in  
 487  $\gamma$  and  $\kappa$  of  $\sqrt{2}(1.58 \text{ ‰})/(119.80 \text{ ‰}) = 0.019$ , also in line with the uncertainties in  $\gamma$  and  $\kappa$ .

488 Rearranging eqns. (24a) and (24b), we obtain expressions for the required  $|\delta_1^{\text{sp}} - \delta_2^{\text{sp}}|$  to  
 489 obtain a target level of uncertainty ( $\sigma$ ) in  $\gamma$  and  $\kappa$ , given the measurement uncertainty in  ${}^{31}R$ :

$$|\delta_1^{\text{sp}} - \delta_2^{\text{sp}}| = \sqrt{2} \frac{\sigma(^{31}\text{R})}{^{15}\text{R}^\alpha} \frac{1}{\sigma_\kappa} \quad (25\text{a})$$

490

$$|\delta_1^{\text{sp}} - \delta_2^{\text{sp}}| = \sqrt{2} \frac{\sigma(^{31}\text{R})}{^{15}\text{R}^\beta} \frac{1}{\sigma_\gamma} \quad (25\text{b})$$

491 Assuming  $\sigma(^{31}\text{R})/^{15}\text{R}^\alpha \approx \sigma(^{31}\text{R})/^{15}\text{R}^\beta \approx \sigma(^{31}\delta)$ , we obtain:

$$|\delta_1^{\text{sp}} - \delta_2^{\text{sp}}| = \sqrt{2} \sigma(^{31}\delta) \frac{1}{\sigma_{\gamma\kappa}} \quad (26)$$

492

493 where  $\sigma(^{31}\delta)$  is the  $^{31}\delta$  measurement uncertainty in per mil, and  $\sigma_{\gamma\kappa}$  is the target absolute  
 494 uncertainty in  $\gamma$  and  $\kappa$ . For example, with a measurement uncertainty of 1 ‰ in  $^{31}\delta$ , the  $\delta(^{15}\text{N}^{\text{sp}})$   
 495 values of the two reference materials must differ by at least 141 ‰ to achieve an absolute  
 496 uncertainty in  $\gamma$  and  $\kappa$  of 0.01. Based on these results, we recommend calculating  $\gamma$  and  $\kappa$  from  
 497 reference materials with a large  $\delta(^{15}\text{N}^{\text{sp}})$  difference, as estimated from eqn. (26).

498 As an alternative to the algebraic solution, a least squares optimization can be used to  
 499 find a solution for  $\gamma$  and  $\kappa$ , although that solution may find a local optimum rather than a global  
 500 optimum. The user can select a least squares optimization instead of the algebraic solution with  
 501 the “method” keyword argument to pyisotopomer’s Scrambling function. The least squares  
 502 optimization smooths measurement uncertainty, making it useful for fitting repeat  
 503 measurements of reference materials to a single pair of “best” values for  $\gamma$  and  $\kappa$ . Its disadvantage  
 504 is that, unlike the algebraic solution, the least squares optimization depends on the initial guess  
 505 for  $\gamma$  and  $\kappa$ . Using data from reference materials CA06261 and CA08214, a range of initial  
 506 guesses from  $\gamma = \kappa = 0.000$  to  $\gamma = \kappa = 0.200$  produced a range of least squares solutions, from  $\gamma =$   
 507  $0.090$  and  $\kappa = 0.000$  to  $\gamma = 0.269$  and  $\kappa = 0.183$  (Figure S3). Despite this range of  $\gamma$  and  $\kappa$ ,  
 508 however, the least squares optimization produced a consistent  $\gamma - \kappa$  of 0.09. As shown in Section  
 509 4.4,  $\gamma - \kappa$  governs the accuracy of  $\delta(^{15}\text{N}^{\text{sp}})$  far more than the individual values of  $\gamma$  and  $\kappa$ .

510 Given an accurate initial guess, the least squares optimization will find a minimum at or  
 511 close to this initial guess, even for reference material pairings close in their  $\delta(^{15}\text{N}^{\text{sp}})$ . For  
 512 example, when we used the algebraic  $\gamma$  and  $\kappa$  from reference materials CA08214 and 53504 as an  
 513 initial guess, the least squares optimization produced similar  $\gamma$  and  $\kappa$  for a variety of reference  
 514 material pairings (Table S2). Furthermore, for the same initial guess, the least squares  
 515 optimization finds different solutions for the Lab 1 and Lab 2 instruments, even for reference  
 516 material pairings close in their  $\delta(^{15}\text{N}^{\text{sp}})$  (Table S3). This demonstrates that, depending on the  
 517 measurement precision at the time, the least squares optimization searches an appropriately wide  
 518 solution space to resolve large differences in instrument behavior.

519 If the first-time user wishes to obtain accurate individual values of  $\gamma$  and  $\kappa$ , we  
 520 recommend obtaining reference materials different enough in their  $\delta(^{15}\text{N}^{\text{sp}})$  to calculate  $\gamma$  and  $\kappa$   
 521 with the algebraic solution. If the user wishes to take advantage of the smoothing of the least  
 522 squares optimization, this algebraic  $\gamma$  and  $\kappa$  can then be used as the initial guess for the least  
 523 squares solver.

524 We also recommend that the user test the accuracy of the least squares  $\gamma$  and  $\kappa$  by  
 525 plugging  $\gamma$  and  $\kappa$  back into eqn. (10) and comparing the result to the measured  $^{31}\text{R}$  for each  
 526 reference material. The two  $^{31}\text{R}$  values should match. pyisotopomer<sup>65</sup> performs this calculation  
 527 automatically and outputs the difference as a  $\delta$  value:

$${}^{31}\delta^{\text{error}} = \frac{{}^{31}R_{\text{calculated}}}{{}^{31}R_{\text{measured}}} - 1 \quad (27)$$

528  
 529 where  ${}^{31}R_{\text{calculated}}$  is calculated by plugging the least squares  $\gamma$  and  $\kappa$  into eqn. (10), and  
 530  ${}^{31}R_{\text{measured}}$  represents the measured  ${}^{31}R$  for each reference material. In the intercalibration  
 531 exercise, the mean of the absolute values of  ${}^{31}\delta^{\text{error}}$  from least squares  $\gamma$  and  $\kappa$  solutions ranged  
 532 from 0.27 ‰ to 0.86 ‰ (Table S2), similar in magnitude to the  ${}^{31}\delta$  analytical uncertainty for  
 533 Labs 1 and 2 (Table S5). This indicates that the amount of error introduced by using the least  
 534 squares optimization is similar to the measurement error in  ${}^{31}\delta$  (Table S2, Table S5). In  
 535 comparison, the  ${}^{31}\delta^{\text{error}}$  introduced by the algebraic solution corresponded to values of  $({}^{31}R_{\text{calculated}}$   
 536  $- {}^{31}R_{\text{measured}})$  within machine precision (Table S2).  
 537

### 538 4.3 Variability in fragmentation behavior

539 As shown above,  $\gamma - \kappa$ , as opposed to the individual values of  $\gamma$  and  $\kappa$ , is the best  
 540 constrained parameter in the scrambling calculation. We show below that  $\gamma - \kappa$  also has the  
 541 greatest impact on  $\delta({}^{15}\text{N}^{\alpha})$ ,  $\delta({}^{15}\text{N}^{\beta})$ , and  $\delta({}^{15}\text{N}^{\text{sp}})$ .  $\gamma - \kappa$  is proportional to  ${}^{31}\delta - {}^{45}\delta$ , and thus is a  
 542 metric of an instrument's scrambling behavior.

543 To examine the change in the fragmentation behavior of a single IRMS over time, we  
 544 compiled values of  $\gamma - \kappa$  for Lab 1 from June 2018 – March 2021 (Figure 3). To equally weigh  
 545 each day of running the instrument, first, we calculated a daily mean  $\gamma - \kappa$ , then calculated a five-  
 546 day running average of  $\gamma - \kappa$  from these daily means. The value of  $\gamma - \kappa$  varied throughout the  
 547 time series, with a mean of  $0.092 \pm 0.002$ . High volatility in  $\gamma - \kappa$  in February-April 2019  
 548 corresponded with a period when the lab temperature was poorly controlled, with strong day-  
 549 night variation (Figure 3). During periods when the lab temperature was stable,  $\gamma - \kappa$  tended to  
 550 increase as the instrument box and trap currents diverged with filament age, although no linear  
 551 relationship emerged.

552 There are several reasons why the scrambling behavior of the ion source might change  
 553 over time, as well as differing between instruments. The  $\text{NO}^+$  fragment ion can be produced by  
 554 one of several routes from  $\text{N}_2\text{O}^+$ <sup>75,76</sup>. The pathways and associated isotope effects for the  
 555 formation of fragment ions are affected by collision frequency, the distribution of excited states,  
 556 and the time spent in the ion source, which suggests that ion source conditions such as vapor  
 557 pressure, ionizing energy, and accelerating voltage may all influence the fragmentation behavior  
 558 of an IRMS system<sup>54,75-78</sup>. Future work could track the effect of variation in these parameters on  
 559 the fragmentation behavior of the instrument, as in Westley et al.<sup>54</sup>, which may allow for  
 560 optimization of fragmentation and scrambling in the ion source.

561 For these reasons, performing the scrambling calibration only once is insufficient to  
 562 obtain high-quality  $\text{N}_2\text{O}$  isotopocule data. Instead, it is important to recalibrate an IRMS system  
 563 for scrambling on a regular basis since ion source conditions may change with time and can shift  
 564 abruptly with events such as filament changes. We recommend using a running average of  $\gamma$  and  
 565  $\kappa$  over a window corresponding to 10 pairings of reference materials, corresponding to a five-day  
 566 window if two pairs of reference materials are run per day. If there is high volatility in  $\gamma$  and  $\kappa$ , as  
 567 seen above in March-April 2019, it may be necessary to shorten this window, to apply  
 568 scrambling corrections most appropriate to instrument conditions.  
 569

### 570 4.4 Sensitivity of position-dependent $\delta$ values to uncertainty in scrambling coefficients



571 The uncertainty in  $\delta(^{15}\text{N}^\alpha)$ ,  $\delta(^{15}\text{N}^\beta)$ , and  $\delta(^{15}\text{N}^{\text{sp}})$  associated with the uncertainty in each  
 572 scrambling coefficient is less straightforward to assess than the uncertainty in  $^{31}\text{R}$  given by eqns.  
 573 (23) and (24), due to the nonlinear relationship between  $\delta(^{15}\text{N}^\alpha)$ ,  $\delta(^{15}\text{N}^\beta)$ ,  $\gamma$ , and  $\kappa$ . (see eqn. (53)  
 574 of Kaiser and Röckmann, 2008). A first order approximation of  $\delta(^{15}\text{N}^{\text{sp}})$  is given by  
 575 (supplementary text S4):

$$\delta(^{15}\text{N}^{\text{sp}}) \approx \frac{2(1 - \gamma + \kappa)}{1 - \gamma - \kappa} ({}^{31}\delta - {}^{45}\delta) \quad (28)$$

576 From this equation, it is apparent that  $\delta(^{15}\text{N}^{\text{sp}})$  is modulated primarily by the difference  $\gamma$   
 577  $-\kappa$ , rather than the individual values of  $\gamma$  and  $\kappa$ . It is also apparent that  $\gamma - \kappa$  is proportional to  ${}^{31}\delta$   
 578  $- {}^{45}\delta$ .

579 A Monte Carlo simulation can be a useful way of visualizing how  $\gamma$ ,  $\kappa$ , and,  $\gamma - \kappa$  impact  
 580  $\delta(^{15}\text{N}^\alpha)$ ,  $\delta(^{15}\text{N}^\beta)$ , and  $\delta(^{15}\text{N}^{\text{sp}})$ . We performed two sensitivity experiments with data from Lab 1:

- 581 1) sensitivity of  $\delta(^{15}\text{N}^\alpha)$ ,  $\delta(^{15}\text{N}^\beta)$ , and  $\delta(^{15}\text{N}^{\text{sp}})$  to  $\gamma - \kappa$ ;
- 582 2) sensitivity of  $\delta(^{15}\text{N}^\alpha)$ ,  $\delta(^{15}\text{N}^\beta)$ , and  $\delta(^{15}\text{N}^{\text{sp}})$  to the individual values of  $\gamma$  and  $\kappa$ , holding  
 583 their difference constant.

584 For the first sensitivity experiment, a Monte Carlo simulation was used to introduce  
 585 random uncertainty in the  $\gamma$  and  $\kappa$  values used to calculate  $\delta$  values of three reference materials.  
 586 Based on Table S2, we chose  $\gamma = 0.174$  and  $\kappa = 0.083$  as central values and varied  $\gamma - \kappa$  such that  
 587 the standard deviation of  $\gamma - \kappa$  was equal to 10 % of the mean (0.091). For the second sensitivity  
 588 experiment, we modeled  $\gamma$  and  $\kappa$  in tandem as random numbers centered around  $\gamma = 0.174$  and  $\kappa =$   
 589  $0.083$ , with uncertainties equal to 10 % of the mean  $\gamma$ , and held  $\gamma - \kappa$  constant at 0.091. For both  
 590 experiments, we sampled 1000 pairs of  $\gamma$  and  $\kappa$ , and then calculated the 1000 simulated values of  
 591  $\delta(^{15}\text{N}^\alpha)$ ,  $\delta(^{15}\text{N}^\beta)$ , and  $\delta(^{15}\text{N}^{\text{sp}})$  for the three reference materials (CA06261, 53504, CA08214).

592 This analysis showed that a 10 % relative uncertainty in  $\gamma - \kappa$  can lead to large variations  
 593 in  $\delta(^{15}\text{N}^\alpha)$ ,  $\delta(^{15}\text{N}^\beta)$ , and  $\delta(^{15}\text{N}^{\text{sp}})$ , e.g., pooled standard deviations of 17.1-18.5 ‰ for  $\delta(^{15}\text{N}^{\text{sp}})$   
 594 (Figure 4a-c). In contrast, a 10 % relative error in  $\gamma$ , keeping  $\gamma - \kappa$  constant, led to pooled  
 595 standard deviations of 1.0-4.3 ‰ in  $\delta(^{15}\text{N}^{\text{sp}})$  (Figure 4d-f). In both experiments, varying  $\gamma$  and  $\kappa$   
 596 produced the most variability for reference material 53504, whose  $\delta(^{15}\text{N}^{\text{sp}})$  was greatest in  
 597 magnitude.

598 These results reflect the earlier conclusion that  $\gamma - \kappa$  is the best constrained parameter in  
 599 the scrambling calculation, and, conversely, that this difference has the greatest effect on  
 600  $\delta(^{15}\text{N}^{\text{sp}})$ . Thus, we recommend regular scrambling calibrations, as assuming the wrong  $\gamma - \kappa$   
 601 difference may have a significant impact on site preferences calculated from these coefficients.  
 602

#### 603 **4.5 Comparison of results between two IRMS laboratories**

604 The application of pyisotopomer was tested through an intercalibration including four  
 605 reference materials and two Lake Lugano samples measured by two IRMS laboratories, plus two  
 606 additional reference materials run in Lab 1. Using an average  $\gamma$  and  $\kappa$  produced by the algebraic  
 607 method from the pairing of reference materials 53504 and CA08214, isotopomers were  
 608 calculated for lake water unknowns, four reference materials run as unknowns for quality  
 609 control, and the two reference materials used in the calibration and (Table 2). This exercise was  
 610 repeated, calculating  $\gamma$  and  $\kappa$  instead with least squares method and the pairing of reference  
 611 materials CA06261 and CA08214 (Table S4). The root mean square deviation (RMSD) for each  
 612 reference material was calculated by comparison to the calibrated values provided by a previous  
 613 intercalibration effort<sup>56</sup> (for atmosphere-equilibrated seawater), an internal standard (B6), and  
 614 four gases sourced from J. Mohn (S2, CA06261, 53504, and CA08214). Almost all isotopomer

615 values produced by the least squares optimization (Table S4) were within error of those produced  
616 by the algebraic solution (Table 2); the latter is discussed below.

617 The  $\delta(^{15}\text{N}^{\text{bulk}})$  measured by the two labs displayed good agreement for each of the four  
618 reference materials, as well as the lake water samples. The  $\delta(^{15}\text{N}^{\text{bulk}})$  RMSDs ranged from 0.2 to  
619 0.6 ‰ (Table 2), all of which were smaller than the 0.8 ‰ presented for IRMS labs by Mohn et  
620 al., (2014). The RMSD for atmospheric  $\text{N}_2\text{O}$  was highest, at 0.6 ‰. For both lake water samples,  
621 the  $\delta(^{15}\text{N}^{\text{bulk}})$  values measured by Lab 1 and Lab 2 were statistically indistinguishable (Table 2;  
622 Figure S4). Likewise, the  $\delta(^{18}\text{O})$  measured by the two labs displayed good agreement for each of  
623 the four reference materials measured by both labs, as well as the lake water samples. The  $\delta(^{18}\text{O})$   
624 RMSDs were slightly greater than the 1.00 ‰ presented for IRMS labs by Mohn et al. (2014),  
625 ranging from 0.5 ‰–1.7 ‰, with the greatest RMSD for reference material 53504 (Table 2). For  
626 the lake water unknowns, the  $\delta(^{18}\text{O})$  values measured by the two labs were within error of each  
627 other (Table 2; Figure S4).

628 The  $\delta(^{15}\text{N}^{\alpha})$  measured by the two labs also showed good agreement for reference  
629 materials CA06261, CA08214, and atmosphere-equilibrated seawater: in each case, the  
630 combined RMSD was less than 2.4 ‰ (Table 2). This is similar to the data presented in Mohn et  
631 al. (2014), who find an RMSD for  $\delta(^{15}\text{N}^{\alpha})$  for IRMS laboratories of 2.47 ‰. The  $\delta(^{15}\text{N}^{\alpha})$   
632 measured by Lab 1 for reference material 53504 ( $0.0 \pm 1.0$  ‰) was lower than both the calibrated  
633 value (1.71 ‰) and the value measured by Lab 2 ( $1.7 \pm 1.0$  ‰). The values of  $\delta(^{15}\text{N}^{\alpha})$  measured  
634 by the two labs for the two lake water samples, however, were within error of each other. For  
635  $\delta(^{15}\text{N}^{\beta})$ , the RMSDs for each reference material were of a similar order of magnitude to  $\delta(^{15}\text{N}^{\alpha})$ ,  
636 ranging from 0.2 ‰–2.1 ‰, similar to the value 2.12 ‰ reported by Mohn et al. (2014). The  
637  $\delta(^{15}\text{N}^{\beta})$  measured by Lab 1 for the lake water unknowns was within error of that measured by  
638 Lab 2 (Table 2; Figure S4). Of note, the  $\delta(^{15}\text{N}^{\beta})$  for the lake water unknown taken at 90 m depth  
639 was  $-32.8$  ‰ (average of measurements by Lab 1 and Lab 2), which is far more negative than  
640 most values observed previously<sup>26,31</sup>.

641 The  $\delta(^{15}\text{N}^{\text{sp}})$  values measured by the two laboratories showed larger standard deviations  
642 than the  $\delta(^{15}\text{N}^{\alpha})$  and  $\delta(^{15}\text{N}^{\beta})$  individually, which is to be expected, since  $\delta(^{15}\text{N}^{\text{sp}})$  is a measure of  
643 difference between the latter two parameters. The  $\delta(^{15}\text{N}^{\text{sp}})$  RMSD values, however, were all less  
644 than 3 ‰ for atmosphere-equilibrated seawater, 53504, and CA08214 (Table 2). This represents  
645 an improvement on Mohn et al. (2014), who find an RMSD of 4.29 ‰ for  $\delta(^{15}\text{N}^{\text{sp}})$  measured by  
646 IRMS laboratories. The  $\delta(^{15}\text{N}^{\text{sp}})$  RMSD for reference material CA06261 was greater, at 4.4 ‰,  
647 which may result from this reference material having a more negative  $\delta(^{15}\text{N}^{\alpha})$  than either of the  
648 two reference materials used in the scrambling calibration. The lake water samples showed larger  
649 offsets in  $\delta(^{15}\text{N}^{\text{sp}})$  than the reference materials (Figure S4). The lake water sample from 10 m  
650 depth showed an especially large difference in  $\delta(^{15}\text{N}^{\text{sp}})$  between Lab 1 and Lab 2: Lab 1  
651 measured a mean  $\delta(^{15}\text{N}^{\text{sp}})$  of  $(18.8 \pm 1.6)$  ‰ at this depth, while Lab 2 measured a mean  $\delta(^{15}\text{N}^{\text{sp}})$   
652 of  $(21.4 \pm 2.5)$  ‰ (Table 2). At 90 m depth, Lab 1 measured a mean  $\delta(^{15}\text{N}^{\text{sp}})$  of  $52.3 \pm 1.2$  ‰, and  
653 Lab 2 measured a mean  $\delta(^{15}\text{N}^{\text{sp}})$  of  $(50.9 \pm 0.5)$  ‰.

654 After size correction and scale normalization, the only consistent difference between  
655 measurements made by the two labs were differences in peak area, which may reflect differences  
656 in the setup of the purge and trap system and/or differences in instrument sensitivity. The  $\text{N}_2\text{O}$   
657 amounts (in nmol) measured in the lake water samples were also similar between the two labs  
658 involved in the intercalibration exercise, indicating that this difference in sensitivity was  
659 adequately compensated for by the peak area to amount conversion factor. In the sample taken at  
660 10 m depth, Lab 1 found  $(2.97 \pm 0.04)$  nmol; Lab 2 found  $(2.31 \pm 0.09)$  nmol. At 90 m depth, Lab 1

661 found (20.46±0.37) nmol; Lab 2 found (19.82±0.01) nmol N<sub>2</sub>O. The intercalibration is expressed  
662 in terms of N<sub>2</sub>O amounts instead of concentrations to eliminate uncertainties in sample volume;  
663 all bottle volumes were the same. Thus, we conclude that differences in sample pretreatment  
664 procedure were corrected for by the size correction and scale normalization steps, leaving no  
665 residual effect on the final  $\delta$  values or N<sub>2</sub>O amounts.

#### 666 **4.6 Additional considerations**

667 The pyisotopomer package produces good results if each of the data preprocessing steps  
668 properly account for size- and delta-dependent effects on the measured isotope ratios <sup>31</sup> $\delta$ , <sup>45</sup> $\delta$ , and  
669 <sup>46</sup> $\delta$ . However, it will produce spurious results under the following circumstances. Firstly, varying  
670 blanks may introduce errors due to the size correction not being applicable to samples and  
671 reference materials alike. Second, if the <sup>45</sup> $\delta$  and <sup>46</sup> $\delta$  scale normalization slope and intercept differ  
672 substantially from one and zero (such as a negative slope), there likely exists an issue with the  
673 scale normalization (such as the reference materials not spanning a wide enough range in <sup>45</sup> $\delta$  and  
674 <sup>46</sup> $\delta$ ). A spurious scale normalization will likewise produce errors in the final isotopocule values.  
675 Thirdly, if reference materials that are too close in their site preferences are used to determine  $\gamma$   
676 and  $\kappa$  with the algebraic solution, the resulting coefficients may represent "unphysical" values  
677 (i.e., not between 0 and 1); these, however, would be inconsequential if the unknown samples  
678 have  $\delta(^{15}\text{N}^{\text{sp}})$  values close to these reference materials. Finally,  $\delta(^{17}\text{O})$  is calculated from a mass  
679 dependent relationship with  $\delta(^{18}\text{O})$  (the parameters of which can be adjusted with keyword  
680 arguments to the Scrambling and Isotopomers functions) unless  $\Delta(^{17}\text{O})$  is determined  
681 separately<sup>60,62,63</sup> and entered in the data corrections template.

#### 682 **5. Conclusion: How to obtain high-quality N<sub>2</sub>O isotopocule data using pyisotopomer**

683 Using pyisotopomer and three reference materials, one can characterize the scrambling  
684 behavior for a given IRMS and apply those scrambling coefficients to calculate the isotopocule  
685 values of unknown samples. To ensure high-quality results from these calculations, we provide  
686 the following recommendations. Firstly, if reference materials with suitably distinct site  
687 preferences are available, we recommend calculating the scrambling coefficients  $\gamma$  and  $\kappa$  from  
688 algebraic solution of eqns. (11) and (12), which is the default method in the Scrambling function  
689 of pyisotopomer. We offer the least squares approach as an alternative, with the following  
690 caveats: 1) The least squares solver finds a minimum close to the initial guess for  $\gamma$  and  $\kappa$ . As  
691 such, if the solver is fed an initial guess other than the absolute minimum calculated from the  
692 algebraic solution, it will find the "wrong" absolute value of  $\gamma$  and  $\kappa$ . It will, however, find the  
693 correct value of  $\gamma - \kappa$ , which has a much larger impact on calculated isotopocules. 2) Using the  
694 "wrong" scrambling coefficients will have only a small effect if the unknowns are close in their  
695  $\delta(^{15}\text{N}^{\alpha})$ ,  $\delta(^{15}\text{N}^{\beta})$ , and  $\delta(^{15}\text{N}^{\text{sp}})$  to those of the reference materials but will have a deleterious effect  
696 as the unknowns diverge in their isotopomer values from the reference materials. 3) If an initial  
697 guess is available, such as through a calibration with the algebraic solution, this should be used  
698 as the initial guess for the least squares solver. Otherwise, we recommend iterating through the  
699 scrambling calculation twice, using the solution from the first iteration as the initial guess for  
700 subsequent calculations. It is necessary to run paired reference materials daily to obtain accurate  
701 running estimates of  $\gamma$  and  $\kappa$ . It is recommended to convert these daily estimates to a one-week  
702 running average and use that average to calculate the isotopocules of unknown samples.

703 Using pyisotopomer in an intercalibration exercise and implementing the above  
704 recommendations, we find good agreement between the calibrated  $\delta$  values measured by two

707 different IRMS labs for both reference materials and natural lake samples. We conclude that  
708 while the intercalibration results demonstrate potential for further improvement in precision, the  
709 intercalibration of  $\delta(^{15}\text{N}^{\text{sp}})$  using a uniform scrambling calculation (pyisotopomer) presented here  
710 represents an improvement upon previous  $\text{N}_2\text{O}$  intercalibrations.

711 In this paper, we demonstrate the need to support efforts to generate and distribute  
712 reference gases to the community. At present, the only commercially available reference  
713 materials are USGS 51 and USGS 52<sup>55</sup>, which do not have sufficiently distinct values of  $\delta(^{15}\text{N}^{\text{sp}})$   
714 to obtain precise values of  $\gamma$  and  $\kappa$  with the algebraic solution unless the user is able to achieve  
715 extremely small measurement uncertainties in  $^{31}\text{R}$ . There have been other efforts to produce  
716 more calibrated  $\text{N}_2\text{O}$  reference gases<sup>79</sup>, but these gases are not yet commercially available. A  
717 fully funded program is needed to produce reference materials such as 53504, which —  
718 combined with reference materials such as USGS 51 and USGS 52 — should provide users with  
719 precise and accurate  $\text{N}_2\text{O}$  isotopocule calibrations.

720

### 721 **Data availability statement**

722 The manuscript is prepared to comply with the RCMS data policy. The latest version of  
723 pyisotopomer is available for installation via the Python Package index  
724 ([pypi.org/project/pyisotopomer](https://pypi.org/project/pyisotopomer)). The second release of pyisotopomer is also available via  
725 Zenodo ([doi.org/10.5281/zenodo.7552724](https://doi.org/10.5281/zenodo.7552724)). This research was supported by U.S.-NSF grant  
726 OCE-1657868 to K. L. Casciotti. C. L. Kelly is supported by an NSF Graduate Research  
727 Fellowship. The authors declare no competing financial interests.

728 **References**

- 729
- 730 1. Yung YL, Wang WC, Lacis AA. Greenhouse effect due to atmospheric nitrous oxide.  
731 *Geophys Res Lett.* 1976;3(10):619-621. doi:10.1029/GL003i010p00619
- 732 2. Smith C, Nicholls ZRJ, Armour K, et al. The Earth's Energy Budget, Climate Feedbacks,  
733 and Climate Sensitivity Supplementary Material. In: Masson-Delmotte V, Zhai P, Pirani A,  
734 et al., eds. *Climate Change 2021: The Physical Science Basis. Contribution of Working*  
735 *Group I to the Sixth Assessment Report of the Intergovernmental Panel on Climate Change.*  
736 Cambridge University Press; 2021. Accessed October 4, 2021.  
737 [https://www.ipcc.ch/report/ar6/wg1/downloads/report/IPCC\\_AR6\\_WGI\\_Chapter\\_07\\_Sup](https://www.ipcc.ch/report/ar6/wg1/downloads/report/IPCC_AR6_WGI_Chapter_07_Supplementary_Material.pdf)  
738 [plementary\\_Material.pdf](https://www.ipcc.ch/report/ar6/wg1/downloads/report/IPCC_AR6_WGI_Chapter_07_Supplementary_Material.pdf)
- 739 3. Crutzen PJ. The influence of nitrogen oxides on the atmospheric ozone content. *Q J R*  
740 *Meteorol Soc.* 1970;96(408):320-325. doi:10.1002/qj.49709640815
- 741 4. Ravishankara AR, Daniel JS, Portmann RW. Nitrous Oxide (N<sub>2</sub>O): The Dominant Ozone-  
742 Depleting Substance Emitted in the 21st Century. *Science.* 2009;326(5949):123-125.  
743 doi:10.1126/science.1176985
- 744 5. Wuebbles DJ. Nitrous Oxide: No Laughing Matter. *Science.* 2009;326(5949):56-57.  
745 doi:10.1126/science.1179571
- 746 6. Müller R. The impact of the rise in atmospheric nitrous oxide on stratospheric ozone.  
747 *Ambio.* 2021;50(1):35-39. doi:10.1007/s13280-020-01428-3
- 748 7. Kim KR, Craig H. Nitrogen-15 and Oxygen-18 Characteristics of Nitrous Oxide: A Global  
749 Perspective. *Science.* 1993;262(5141):1855-1857. doi:10.1126/science.262.5141.1855
- 750 8. Pérez T, Trumbore SE, Tyler SC, Davidson EA, Keller M, Camargo PB de. Isotopic  
751 variability of N<sub>2</sub>O emissions from tropical forest soils. *Glob Biogeochem Cycles.*  
752 2000;14(2):525-535. doi:10.1029/1999GB001181
- 753 9. Kim KR, Craig H. Two-isotope characterization of N<sub>2</sub>O in the Pacific Ocean and  
754 constraints on its origin in deep water. *Nature.* 1990;347(6288):58-61.  
755 doi:10.1038/347058a0
- 756 10. Dore JE, Popp BN, Karl DM, Sansone FJ. A large source of atmospheric nitrous oxide from  
757 subtropical North Pacific surface waters. *Nature.* 1998;396(6706):63-66.  
758 doi:10.1038/23921
- 759 11. Naqvi SWA, Naik H, Jayakumar A, et al. Seasonal Anoxia Over the Western Indian  
760 Continental Shelf. In: Wiggert JD, Hood RR, Naqvi SWA, Brink KH, Smith SL, eds.  
761 *Geophysical Monograph Series.* Vol 185. American Geophysical Union; 2009:333-345.  
762 doi:10.1029/2008GM000745
- 763 12. Yoshida N, Hattori A, Saino T, Matsuo S, Wada E. 15N/14N ratio of dissolved N<sub>2</sub>O in the  
764 eastern tropical Pacific Ocean. *Nature.* Published online 1984. doi:10.1038/307442A0

- 765 13. Rahn T, Wahlen M. Stable Isotope Enrichment in Stratospheric Nitrous Oxide. *Science*.  
766 1997;278(5344):1776-1778. doi:10.1126/science.278.5344.1776
- 767 14. Rahn T, Wahlen M. A reassessment of the global isotopic budget of atmospheric nitrous  
768 oxide. *Glob Biogeochem Cycles*. 2000;14(2):537-543. doi:10.1029/1999GB900070
- 769 15. Yoshida N. <sup>15</sup>N-depleted N<sub>2</sub>O as a product of nitrification. *Nature*. 1988;335(6190):528-  
770 529. doi:10.1038/335528a0
- 771 16. Barford CC, Montoya JP, Altabet MA, Mitchell R. Steady-State Nitrogen Isotope Effects of  
772 N<sub>2</sub> and N<sub>2</sub>O Production in *Paracoccus denitrificans*. *Appl Environ Microbiol*.  
773 1999;65(3):989-994. doi:10.1128/AEM.65.3.989-994.1999
- 774 17. Pérez T, Trumbore SE, Tyler SC, et al. Identifying the agricultural imprint on the global  
775 N<sub>2</sub>O budget using stable isotopes. *J Geophys Res Atmospheres*. 2001;106(D9):9869-9878.  
776 doi:10.1029/2000JD900809
- 777 18. Yamulki S, Toyoda S, Yoshida N, Veldkamp E, Grant B, Bol R. Diurnal fluxes and the  
778 isotopomer ratios of N<sub>2</sub>O in a temperate grassland following urine amendment. *Rapid*  
779 *Commun Mass Spectrom*. 2001;15(15):1263-1269. doi:10.1002/rcm.352
- 780 19. Lewicka-Szczebak D, Augustin J, Gieseemann A, Well R. Quantifying N<sub>2</sub>O reduction to N<sub>2</sub>  
781 based on N<sub>2</sub>O isotopocules – validation with independent methods (helium incubation and  
782 <sup>15</sup>N gas flux method). *Biogeosciences*. 2017;14(3):711-732. doi:https://doi.org/10.5194/bg-  
783 14-711-2017
- 784 20. Verhoeven E, Barthel M, Yu L, et al. Early season N<sub>2</sub>O emissions under variable water  
785 management in rice systems: source-partitioning emissions using isotope ratios along a  
786 depth profile. *Biogeosciences*. 2019;16(2):383-408. doi:https://doi.org/10.5194/bg-16-383-  
787 2019
- 788 21. Yoshida N, Toyoda S. Constraining the atmospheric N<sub>2</sub>O budget from intramolecular site  
789 preference in N<sub>2</sub>O isotopomers. *Nature*. 2000;405(6784):330-334. doi:10.1038/35012558
- 790 22. Prokopiou M, Martinerie P, Link to external site this link will open in a new window, et al.  
791 Constraining N<sub>2</sub>O emissions since 1940 using firm air isotope measurements in both  
792 hemispheres. *Atmospheric Chem Phys*. 2017;17(7):4539-4564. doi:10.5194/acp-17-4539-  
793 2017
- 794 23. Yu L, Harris E, Henne S, et al. The isotopic composition of atmospheric nitrous oxide  
795 observed at the high-altitude research station Jungfrauoch, Switzerland. *Atmospheric Chem*  
796 *Phys*. 2020;20(11):6495-6519. doi:10.5194/acp-20-6495-2020
- 797 24. Toyoda S, Yoshida N, Miwa T, et al. Production mechanism and global budget of N<sub>2</sub>O  
798 inferred from its isotopomers in the western North Pacific. *Geophys Res Lett*. 2002;29(3):7-  
799 1-7-4. doi:10.1029/2001GL014311

- 800 25. Popp BN, Westley MB, Toyoda S, et al. Nitrogen and oxygen isotopomeric constraints on  
801 the origins and sea-to-air flux of N<sub>2</sub>O in the oligotrophic subtropical North Pacific gyre.  
802 *Glob Biogeochem Cycles*. 2002;16(4):12-1-12-10. doi:10.1029/2001GB001806
- 803 26. Yamagishi H, Westley MB, Popp BN, et al. Role of nitrification and denitrification on the  
804 nitrous oxide cycle in the eastern tropical North Pacific and Gulf of California. *J Geophys*  
805 *Res Biogeosciences*. 2007;112(G2). doi:10.1029/2006JG000227
- 806 27. Yamagishi H, Yoshida N, Toyoda S, Popp BN, Westley MB, Watanabe S. Contributions of  
807 denitrification and mixing on the distribution of nitrous oxide in the North Pacific. *Geophys*  
808 *Res Lett*. 2005;32(4). doi:10.1029/2004GL021458
- 809 28. Westley MB, Yamagishi H, Popp BN, Yoshida N. Nitrous oxide cycling in the Black Sea  
810 inferred from stable isotope and isotopomer distributions. *Deep Sea Res Part II Top Stud*  
811 *Oceanogr*. 2006;53(17-19):1802-1816. doi:10.1016/j.dsr2.2006.03.012
- 812 29. Farías L, Castro-González M, Cornejo M, et al. Denitrification and nitrous oxide cycling  
813 within the upper oxycline of the eastern tropical South Pacific oxygen minimum zone.  
814 *Limnol Oceanogr*. 2009;54(1):132-144. doi:10.4319/lo.2009.54.1.0132
- 815 30. Casciotti KL, Forbes M, Vedamati J, Peters BD, Martin TS, Mordy CW. Nitrous oxide  
816 cycling in the Eastern Tropical South Pacific as inferred from isotopic and isotopomeric  
817 data. *Deep Sea Res Part II Top Stud Oceanogr*. 2018;156:155-167.  
818 doi:10.1016/j.dsr2.2018.07.014
- 819 31. Bourbonnais A, Letscher RT, Bange HW, et al. N<sub>2</sub>O production and consumption from  
820 stable isotopic and concentration data in the Peruvian coastal upwelling system. *Glob*  
821 *Biogeochem Cycles*. 2017;31(4):678-698. doi:10.1002/2016GB005567
- 822 32. Toyoda S, Yoshida O, Yamagishi H, Fujii A, Yoshida N, Watanabe S. Identifying the  
823 origin of nitrous oxide dissolved in deep ocean by concentration and isotopocule analyses.  
824 *Sci Rep*. 2019;9(1):1-9. doi:10.1038/s41598-019-44224-0
- 825 33. Kelly CL, Travis NM, Baya PA, Casciotti KL. Quantifying Nitrous Oxide Cycling Regimes  
826 in the Eastern Tropical North Pacific Ocean With Isotopomer Analysis. *Glob Biogeochem*  
827 *Cycles*. 2021;35(2):e2020GB006637. doi:10.1029/2020GB006637
- 828 34. Toyoda S, Kakimoto T, Kudo K, et al. Distribution and Production Mechanisms of N<sub>2</sub>O in  
829 the Western Arctic Ocean. *Glob Biogeochem Cycles*. 2021;35(4):e2020GB006881.  
830 doi:https://doi.org/10.1029/2020GB006881
- 831 35. Friedman L, Bigeleisen J. Oxygen and Nitrogen Isotope Effects in the Decomposition of  
832 Ammonium Nitrate. *J Chem Phys*. 1950;18(10):1325-1331. doi:10.1063/1.1747471
- 833 36. Toyoda S, Yoshida N. Determination of nitrogen isotopomers of nitrous oxide on a  
834 modified isotope ratio mass spectrometer. *Anal Chem*. 1999;71(20):4711-4718.  
835 doi:10.1021/ac9904563

- 836 37. Brenninkmeijer CAM, Röckmann T. Mass spectrometry of the intramolecular nitrogen  
837 isotope distribution of environmental nitrous oxide using fragment-ion analysis. *Rapid*  
838 *Commun Mass Spectrom.* 1999;13(20):2028-2033. doi:10.1002/(SICI)1097-  
839 0231(19991030)13:20<2028::AID-RCM751>3.0.CO;2-J
- 840 38. Kaiser J, Brenninkmeijer CAM, Röckmann T. Intramolecular <sup>15</sup>N and <sup>18</sup>O fractionation in  
841 the reaction of N<sub>2</sub>O with O(<sup>1</sup>D) and its implications for the stratospheric N<sub>2</sub>O isotope  
842 signature. *J Geophys Res Atmospheres.* 2002;107(D14):ACH 16-1-ACH 16-14.  
843 doi:10.1029/2001JD001506
- 844 39. Kaiser J. *Stable Isotope Investigations of Atmospheric Nitrous Oxide.* Johannes Gutenberg  
845 University of Mainz; 2003. <https://doi.org/10.25358/openscience-3976>
- 846 40. Röckmann T, Levin I. High-precision determination of the changing isotopic composition  
847 of atmospheric N<sub>2</sub>O from 1990 to 2002. *J Geophys Res Atmospheres.* 2005;110(D21).  
848 doi:10.1029/2005JD006066
- 849 41. Yung YL, Miller CE. Isotopic Fractionation of Stratospheric Nitrous Oxide. *Science.*  
850 1997;278(5344):1778-1780. doi:10.1126/science.278.5344.1778
- 851 42. Röckmann T, Kaiser J, Brenninkmeijer CAM, et al. Isotopic enrichment of nitrous oxide  
852 (<sup>15</sup>N<sup>14</sup>NO, <sup>14</sup>N<sup>15</sup>NO, <sup>14</sup>N<sup>14</sup>N<sup>18</sup>O) in the stratosphere and in the laboratory. *J Geophys*  
853 *Res Atmospheres.* 2001;106(D10):10403-10410. doi:10.1029/2000JD900822
- 854 43. Toyoda S, Yoshida N, Urabe T, et al. Temporal and latitudinal distributions of stratospheric  
855 N<sub>2</sub>O isotopomers. *J Geophys Res Atmospheres.* 2004;109(D8). doi:10.1029/2003JD004316
- 856 44. Kaiser J, Engel A, Borchers R, Rockmann T. Probing stratospheric transport and chemistry  
857 with new balloon and aircraft observations of the meridional and vertical N<sub>2</sub>O isotope  
858 distribution. *Atmos Chem Phys.* Published online 2006:22.
- 859 45. Park S, Atlas EL, Boering KA. Measurements of N<sub>2</sub>O isotopologues in the stratosphere:  
860 Influence of transport on the apparent enrichment factors and the isotopologue fluxes to the  
861 troposphere. *J Geophys Res Atmospheres.* 2004;109(D1). doi:10.1029/2003JD003731
- 862 46. Sutka RL, Ostrom NE, Ostrom PH, Gandhi H, Breznak JA. Nitrogen isotopomer site  
863 preference of N<sub>2</sub>O produced by *Nitrosomonas europaea* and *Methylococcus capsulatus*  
864 Bath. *Rapid Commun Mass Spectrom RCM.* 2003;17(7):738-745. doi:10.1002/rcm.968
- 865 47. Sutka RL, Ostrom NE, Ostrom PH, et al. Distinguishing Nitrous Oxide Production from  
866 Nitrification and Denitrification on the Basis of Isotopomer Abundances. *Appl Environ*  
867 *Microbiol.* 2006;72(1):638-644. doi:10.1128/AEM.72.1.638-644.2006
- 868 48. Sutka RL, Ostrom NE, Ostrom PH, Gandhi H, Breznak JA. Nitrogen isotopomer site  
869 preference of N<sub>2</sub>O produced by *Nitrosomonas europaea* and *Methylococcus capsulatus*  
870 Bath. *Rapid Commun Mass Spectrom.* 2004;18(12):1411-1412. doi:10.1002/rcm.1482



- 871 49. Toyoda S, Mutobe H, Yamagishi H, Yoshida N, Tanji Y. Fractionation of N<sub>2</sub>O isotopomers  
872 during production by denitrifier. *Soil Biol Biochem.* 2005;37(8):1535-1545.  
873 doi:10.1016/j.soilbio.2005.01.009
- 874 50. Frame CH, Casciotti KL. Biogeochemical controls and isotopic signatures of nitrous oxide  
875 production by a marine ammonia-oxidizing bacterium. *Biogeosciences.* 2010;7(9):2695-  
876 2709. doi:10.5194/bg-7-2695-2010
- 877 51. Lazo-Murphy BM, Larson S, Staines S, et al. Nitrous oxide production and isotopomer  
878 composition by fungi isolated from salt marsh sediments. *Front Mar Sci.* 2022;9. Accessed  
879 January 3, 2023. <https://www.frontiersin.org/articles/10.3389/fmars.2022.1098508>
- 880 52. Ostrom NE, Pitt A, Sutka R, et al. Isotopologue effects during N<sub>2</sub>O reduction in soils and in  
881 pure cultures of denitrifiers. *J Geophys Res Biogeosciences.* 2007;112(G2).  
882 doi:10.1029/2006JG000287
- 883 53. Kaiser J, Park S, Boering KA, Brenninkmeijer CAM, Hilker A, Röckmann T. Mass  
884 spectrometric method for the absolute calibration of the intramolecular nitrogen isotope  
885 distribution in nitrous oxide. *Anal Bioanal Chem.* 2004;378(2):256-269.  
886 doi:10.1007/s00216-003-2233-2
- 887 54. Westley MB, Popp BN, Rust TM. The calibration of the intramolecular nitrogen isotope  
888 distribution in nitrous oxide measured by isotope ratio mass spectrometry. *Rapid Commun*  
889 *Mass Spectrom.* 2007;21(3):391-405. doi:10.1002/rcm.2828
- 890 55. Ostrom NE, Gandhi H, Coplen TB, et al. Preliminary assessment of stable nitrogen and  
891 oxygen isotopic composition of USGS51 and USGS52 nitrous oxide reference gases and  
892 perspectives on calibration needs. *Rapid Commun Mass Spectrom.* 2018;32(15):1207-1214.  
893 doi:10.1002/rcm.8157
- 894 56. Mohn J, Wolf B, Toyoda S, et al. Interlaboratory assessment of nitrous oxide isotopomer  
895 analysis by isotope ratio mass spectrometry and laser spectroscopy: current status and  
896 perspectives. *Rapid Commun Mass Spectrom.* 2014;28(18):1995-2007.  
897 doi:10.1002/rcm.6982
- 898 57. Kelly CL. pyisotopomer: Nitrous oxide isotopomer data corrections in Python. Published  
899 online January 5, 2023. Accessed March 13, 2023. <https://pypi.org/project/pyisotopomer/>
- 900 58. Baertschi P. Absolute <sup>18</sup>O content of standard mean ocean water. *Earth Planet Sci Lett.*  
901 1976;31(3):341-344. doi:10.1016/0012-821X(76)90115-1
- 902 59. Jabeen I, Kusakabe M. Determination of δ <sup>17</sup>O values of reference water samples VSMOW  
903 and SLAP. *Chem Geol.* 1997;143:115-119. doi:10.1016/S0009-2541(97)00109-5
- 904 60. Kaiser J, Röckmann T, Brenninkmeijer CAM. Complete and accurate mass spectrometric  
905 isotope analysis of tropospheric nitrous oxide. *J Geophys Res Atmospheres.*  
906 2003;108(D15). doi:10.1029/2003JD003613

- 907 61. Kaiser J, Röckmann T. Correction of mass spectrometric isotope ratio measurements for  
908 isobaric isotopologues of O<sub>2</sub>, CO, CO<sub>2</sub>, N<sub>2</sub>O and SO<sub>2</sub>. *Rapid Commun Mass Spectrom.*  
909 2008;22(24):3997-4008. doi:10.1002/rcm.3821
- 910 62. Kaiser J, Hastings MG, Houlton BZ, Röckmann T, Sigman DM. Triple Oxygen Isotope  
911 Analysis of Nitrate Using the Denitrifier Method and Thermal Decomposition of N<sub>2</sub>O.  
912 *Anal Chem.* 2007;79(2):599-607. doi:10.1021/ac061022s
- 913 63. Wankel SD, Ziebis W, Buchwald C, et al. Evidence for fungal and chemodenitrification  
914 based N<sub>2</sub>O flux from nitrogen impacted coastal sediments. *Nat Commun.* 2017;8(1):1-11.  
915 doi:10.1038/ncomms15595
- 916 64. Magyar PM, Orphan VJ, Eiler JM. Measurement of rare isotopologues of nitrous oxide by  
917 high-resolution multi-collector mass spectrometry. *Rapid Commun Mass Spectrom.*  
918 2016;30(17):1923-1940. doi:10.1002/rcm.7671
- 919 65. Kelly CL. ckelly314/pyisotopomer: v1.0.4. Published online January 19, 2023.  
920 doi:10.5281/zenodo.7552724
- 921 66. McIlvin MR, Casciotti KL. Technical updates to the bacterial method for nitrate isotopic  
922 analyses. *Anal Chem.* 2011;83(5):1850-1856. doi:10.1021/ac1028984
- 923 67. McIlvin MR, Casciotti KL. Fully automated system for stable isotopic analyses of dissolved  
924 nitrous oxide at natural abundance levels. *Limnol Oceanogr Methods.* 2010;8(2):54-66.  
925 doi:10.4319/lom.2010.8.54
- 926 68. Scott KM, Lu X, Cavanaugh CM, Liu JS. Optimal methods for estimating kinetic isotope  
927 effects from different forms of the Rayleigh distillation equation 1 Associate editor: J.  
928 Horita. *Geochim Cosmochim Acta.* 2004;68(3):433-442. doi:10.1016/S0016-  
929 7037(03)00459-9
- 930 69. LI W. Measurement of the absolute abundance of oxygen-17 in V-SMOW. *Chin Sci Bull.*  
931 1988;33:1610-1613. Accessed June 10, 2021. <https://ci.nii.ac.jp/naid/80004607415/>
- 932 70. Santoro AE, Buchwald C, McIlvin MR, Casciotti KL. Isotopic Signature of N<sub>2</sub>O Produced  
933 by Marine Ammonia-Oxidizing Archaea. *Science.* 2011;333(6047):1282-1285.  
934 doi:10.1126/science.1208239
- 935 71. Dutton GS, Elkins JW, Hall BD. Nitrous Oxide data from the NOAA/ESRL halocarbons in  
936 situ program. Published online 2021. Accessed November 19, 2021.  
937 <https://data.nodc.noaa.gov/cgi-bin/iso?id=gov.noaa.ncdc:C01556>
- 938 72. Inoue HY, Mook WG. Equilibrium and kinetic nitrogen and oxygen isotope fractionations  
939 between dissolved and gaseous N<sub>2</sub>O. *Chem Geol.* 1994;113(1):135-148. doi:10.1016/0009-  
940 2541(94)90009-4
- 941 73. Röckmann T, Kaiser J, Brenninkmeijer CAM, Brand WA. Gas chromatography/isotope-  
942 ratio mass spectrometry method for high-precision position-dependent <sup>15</sup>N and <sup>18</sup>O

- 943 measurements of atmospheric nitrous oxide. *Rapid Commun Mass Spectrom.*  
944 2003;17(16):1897-1908. doi:10.1002/rcm.1132
- 945 74. Glover DM, Jenkins WJ, Doney SC. *Modeling Methods for Marine Science.* Cambridge  
946 University Press; 2011. doi:10.1017/CBO9780511975721
- 947 75. Lorquet JC, Cadet C. Excited states of gaseous ions: I. Selection rules in photoelectron  
948 spectroscopy and photoionization. The case of N<sub>2</sub>O<sup>+</sup>. *Int J Mass Spectrom Ion Phys.*  
949 1971;7(3):245-254. doi:10.1016/0020-7381(71)80020-7
- 950 76. Märk E, Märk TD, Kim YB, Stephan K. Absolute electron impact ionization cross section  
951 from threshold up to 180 eV for N<sub>2</sub>O+e<sup>-</sup>→N<sub>2</sub>O<sup>++</sup>+2e<sup>-</sup> and the metastable and collision  
952 induced dissociation of N<sub>2</sub>O<sup>+</sup>. *J Chem Phys.* 1981;75(9):4446-4453. doi:10.1063/1.442611
- 953 77. Bigeleisen J. Chemistry of Isotopes. *Science.* 1965;147(3657):463-471.  
954 doi:10.1126/science.147.3657.463
- 955 78. Begun GM, Landau L. Metastable Transitions in N<sub>2</sub>O<sup>+</sup>. *J Chem Phys.* 1962;36(4):1083-  
956 1084. doi:10.1063/1.1732641
- 957 79. Mohn J, Biasi C, Bodé S, et al. Isotopically characterised N<sub>2</sub>O reference materials for use  
958 as community standards. *Rapid Commun Mass Spectrom.* 2022;36(13):e9296.  
959 doi:10.1002/rcm.9296
- 960  
961

962 **Table 1.** Reference materials for N<sub>2</sub>O isotopic analysis and intercalibration. Except for one internal standard (B6),  
 963 calibrated values were provided via independent measurement by S. Toyoda, Tokyo Tech., J. Mohn, EMPA; or, in  
 964 the case of tropospheric N<sub>2</sub>O, the 2018 annual average measured at Jungfraujoch, Switzerland, reported by Yu et al.  
 965 (2020). The laboratories participating in the intercalibration exercise were at Stanford University (“Lab 1”) and the  
 966 University of Basel (“Lab 2”). <sup>31</sup>R values represent the inherent, unscrambled <sup>31</sup>R of each reference material,  
 967 calculated from eqn. (6).

Reference material	Matrix	Mole fraction	$\delta(^{15}\text{N}^\alpha)$	$\delta(^{15}\text{N}^\beta)$	$\delta(^{15}\text{N}^{\text{sp}})$	$\delta(^{15}\text{N}^{\text{bulk}})$	$\delta(^{18}\text{O})$	$^{31}\text{R}$ ( $^{15}\text{R}^\alpha + ^{17}\text{R}$ )	$^{45}\text{R}$	$^{46}\text{R}$	Calibration by	
		$\mu\text{mol mol}^{-1}$	( $\text{‰}$ , vs. <i>air N<sub>2</sub></i> )				( $\text{‰}$ , vs. <i>VSMOW</i> )					
S2 reference gas	Synthetic air	90	5.55	-12.87	18.42	-3.66	32.73	0.004083	0.007712	0.002087	Toyoda & Mohn	
B6 reference gas	He	900	-0.40	-0.15	-0.26	-0.28	41.95	0.004063	0.007739	0.002106	Lab 1 internal standard	
Tropospheric N <sub>2</sub> O (2018 annual average)	Air	~0.33	15.6	-2.3	17.9	6.6	44.4	0.004123	0.007787	0.002111	Yu et al. (2020)	
CA06261	Synthetic air	90	-22.21	-49.28	27.07	-35.75	26.94	0.003980	0.007475	0.002075	Toyoda & Mohn	
53504	Synthetic air	90	1.71	94.44	-92.73	48.08	36.01	0.004070	0.008093	0.002095	Toyoda & Mohn	
CA08214	Synthetic air	90	17.11	-3.43	20.54	6.84	35.39	0.004126	0.007790	0.002093	Toyoda & Mohn	
90454	Synthetic air	90	25.73	25.44	0.29	25.59	35.88	0.004158	0.007928	0.002094	Toyoda & Mohn	
94321	Synthetic air	90	50.52	2.21	48.31	26.37	35.54	0.004249	0.007934	0.002094	Toyoda & Mohn	
Lab 1 pure N <sub>2</sub> O direct injection ("A01")	Pure N <sub>2</sub> O	N/A	0.24	0.12	0.13	0.18	39.85	0.003734	0.007742	0.002101	Toyoda	
Lab 2 pure N <sub>2</sub> O direct injection	Pure N <sub>2</sub> O	N/A	-4.07	3.59	-7.66	-0.24	39.25	0.004044	0.007739	0.002100	Mohn	

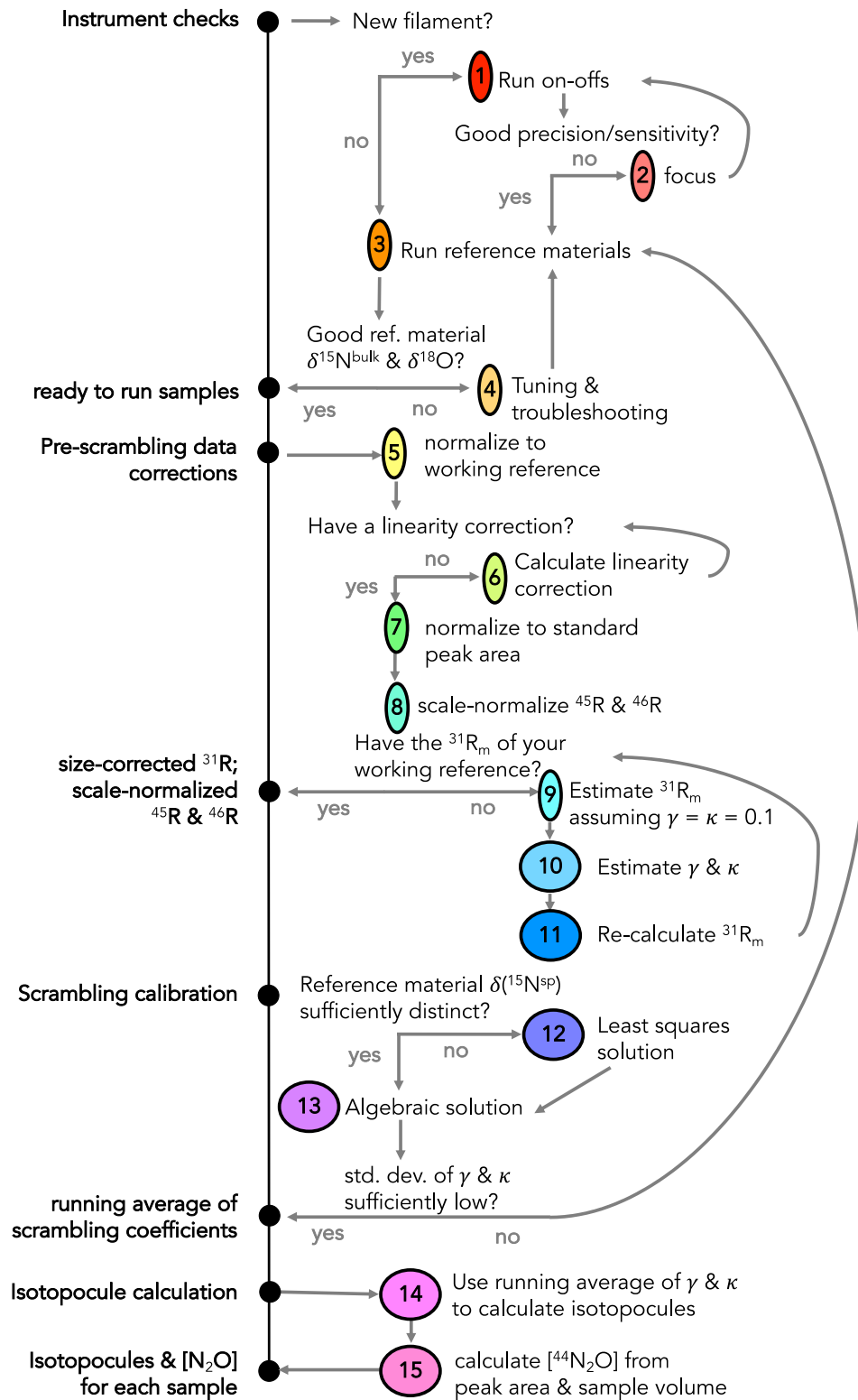
968  
969

970 **Table 2.** N<sub>2</sub>O isotopic composition of reference materials and two unknowns analyzed by two IRMS laboratories,  
 971 calculated using  $\gamma$  and  $\kappa$  values determined from reference materials 53504 and CA08214 with the algebraic  
 972 solution.  $\delta(^{15}\text{N}^\alpha)$ ,  $\delta(^{15}\text{N}^\beta)$ ,  $\delta(^{15}\text{N}^{\text{sp}})$  and  $\delta(^{15}\text{N}^{\text{bulk}})$  are reported in ‰ vs. Air N<sub>2</sub>, and  $\delta(^{18}\text{O})$  is reported in ‰ vs.  
 973 VSMOW. Uncertainties are standard deviations of replicate bottles and do not include calibration uncertainties. The  
 974 root-mean square deviation (RMSD) was calculated with respect to calibrated values.

975

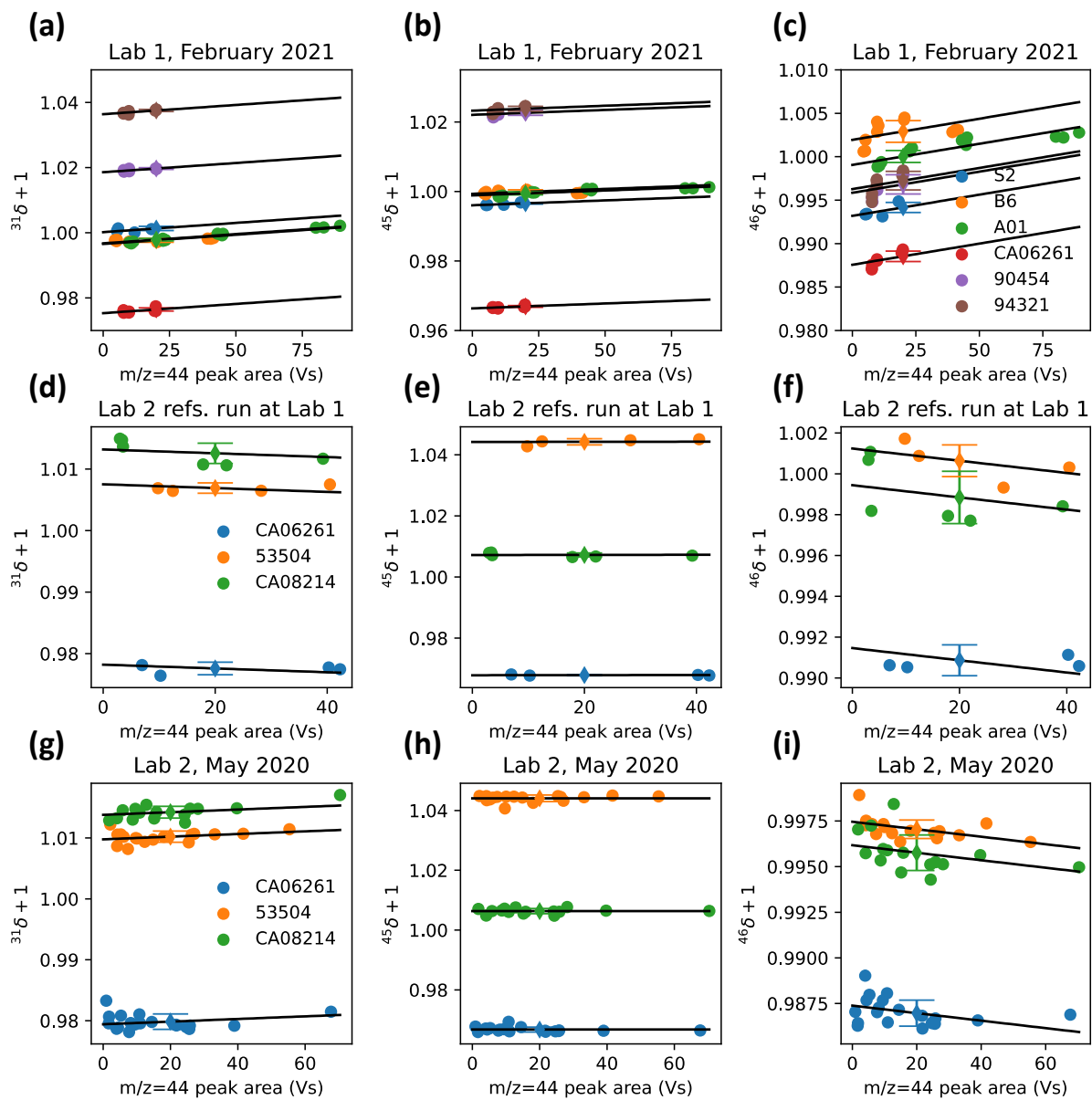
Reference material		<i>n</i>	$\delta(^{15}\text{N}^\alpha)$	$\sigma$	$\delta(^{15}\text{N}^\beta)$	$\sigma$	$\delta(^{15}\text{N}^{\text{sp}})$	$\sigma$	$\delta(^{15}\text{N}^{\text{bulk}})$	$\sigma$	$\delta(^{18}\text{O})$	$\sigma$
			(‰, vs. air N <sub>2</sub> )						(‰, vs. VSMOW)			
CA06261	Calibrated value		-22.2		-49.3		27.1		-35.7		26.9	
	Lab 1	4	-20.6	1.3	-50.5	1.3	29.9	2.7	-35.6	0.2	28.4	0.8
	Lab 2	16	-20.5	1.4	-50.9	2.6	30.4	3.8	-35.7	1.0	27.6	1.8
	RMSD		2.3		2.1		4.4		0.2		1.5	
53504	Calibrated value		1.7		94.4		-92.7		48.1		36.0	
	Lab 1	4	0.0	1.0	95.7	2.1	-95.7	2.5	47.9	1.1	37.6	0.8
	Lab 2	15	1.7	1.0	94.5	1.9	-92.8	2.9	48.1	0.6	36.4	1.6
	RMSD		1.7		1.3		3.0		0.2		1.7	
CA08214	Calibrated value		17.1		-3.4		20.5		6.8		35.3	
	Lab 1	6	17.0	2.0	-2.4	0.9	19.4	2.9	7.3	0.7	36.3	1.4
	Lab 2	16	17.0	1.1	-3.2	0.7	20.2	1.3	6.9	0.6	36.0	3.6
	RMSD		0.1		1.1		1.2		0.5		1.3	
Tropospheric N <sub>2</sub> O	Calibrated value		15.6		-2.3		17.9		6.6		44.4	
	Lab 1	7	15.1	0.8	-2.5	2.3	17.5	2.8	6.3	1.0	43.1	2.1
	Lab 2	2	15.8	1.1	-3.7	0.0	19.5	1.0	6.1	0.5	44.7	1.0
	RMSD		0.6		1.4		1.7		0.6		1.3	
B6	Calibrated value		-0.4		-0.1		-0.3		-0.3		41.9	
	Lab 1	7	-2.2	0.7	1.3	1.0	-3.4	1.2	-0.4	0.7	41.5	1.6
	RMSD		1.8		1.4		3.2		0.2		0.5	
S2	Calibrated value		5.6		-12.9		18.4		-3.7		32.7	
	Lab1	6	5.0	0.5	-13.1	1.6	18.1	1.3	-4.0	1.0	31.5	1.8
	RMSD		0.5		0.2		0.3		0.4		1.2	
Lake Lugano, 10m	Lab 1	3	13.2	0.3	-5.6	1.2	18.8	1.5	3.8	0.4	44.6	1.2
	Lab 2	5	14.8	1.5	-6.6	1.3	21.4	2.5	4.1	0.5	45.5	0.6
Lake Lugano, 90m	Lab 1	3	19.2	0.5	-33.1	0.7	52.3	1.2	-6.9	0.1	56.8	0.1
	Lab 2	2	18.5	0.8	-32.4	0.3	50.9	0.5	-6.9	0.5	55.4	1.9

976



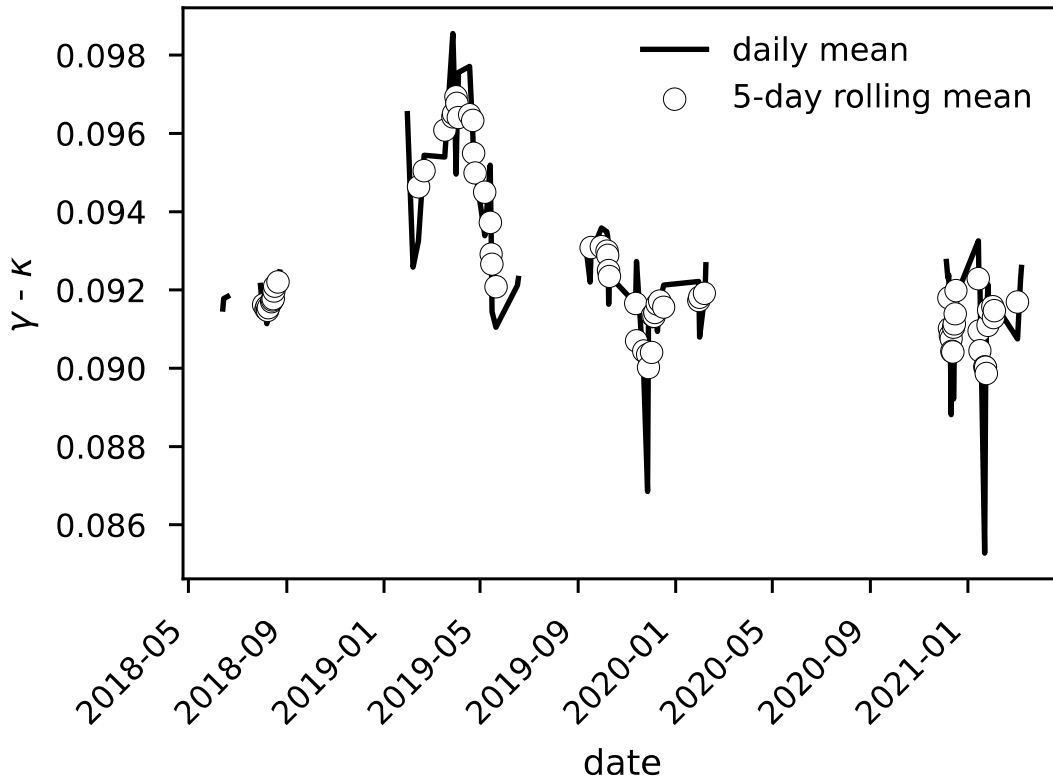
977  
978  
979  
980  
981

**Figure 1.**  $\text{N}_2\text{O}$  data corrections flowchart. Instrument checks, pre-scrambling data corrections, the scrambling calibration, and isotopomer calculations are laid out; numbers in yellow circles correspond to step numbers referred to in the text. Steps 1-4 are performed with raw Isodat output, steps 5-8 are accomplished in the data corrections spreadsheet template, step 9 is a simple calculation, and steps 10-14 are accomplished with the pyisotopomer code.



982  
 983 **Figure 2.** Linearity relations for reference materials used to normalize measured isotope ratios to a peak area of 20  
 984 Vs (10 nmol N<sub>2</sub>O), using the dummy variable method<sup>68</sup>. <sup>31</sup>δ+1 (a,d,g), <sup>45</sup>δ+1 (b,e,h), and <sup>46</sup>δ+1 (c, f, i) are plotted  
 985 against *m/z* 44 peak area. Linearity relations are shown for reference materials prepared and run in Lab 1 (a-c),  
 986 reference materials prepared in Lab 2 but run in Lab 1 (d-f), and reference materials run in Lab 2 (g-i). A common  
 987 slope (black line) calculated from the dummy variable method for each molecular ion ratio is overlain on each data  
 988 series (colored circles). The estimated isotope ratio corresponding to a peak area of 20 Vs/10 nmols N<sub>2</sub>O is also  
 989 shown for each series (colored diamonds, error bars correspond to the standard error of the predicted y-value).

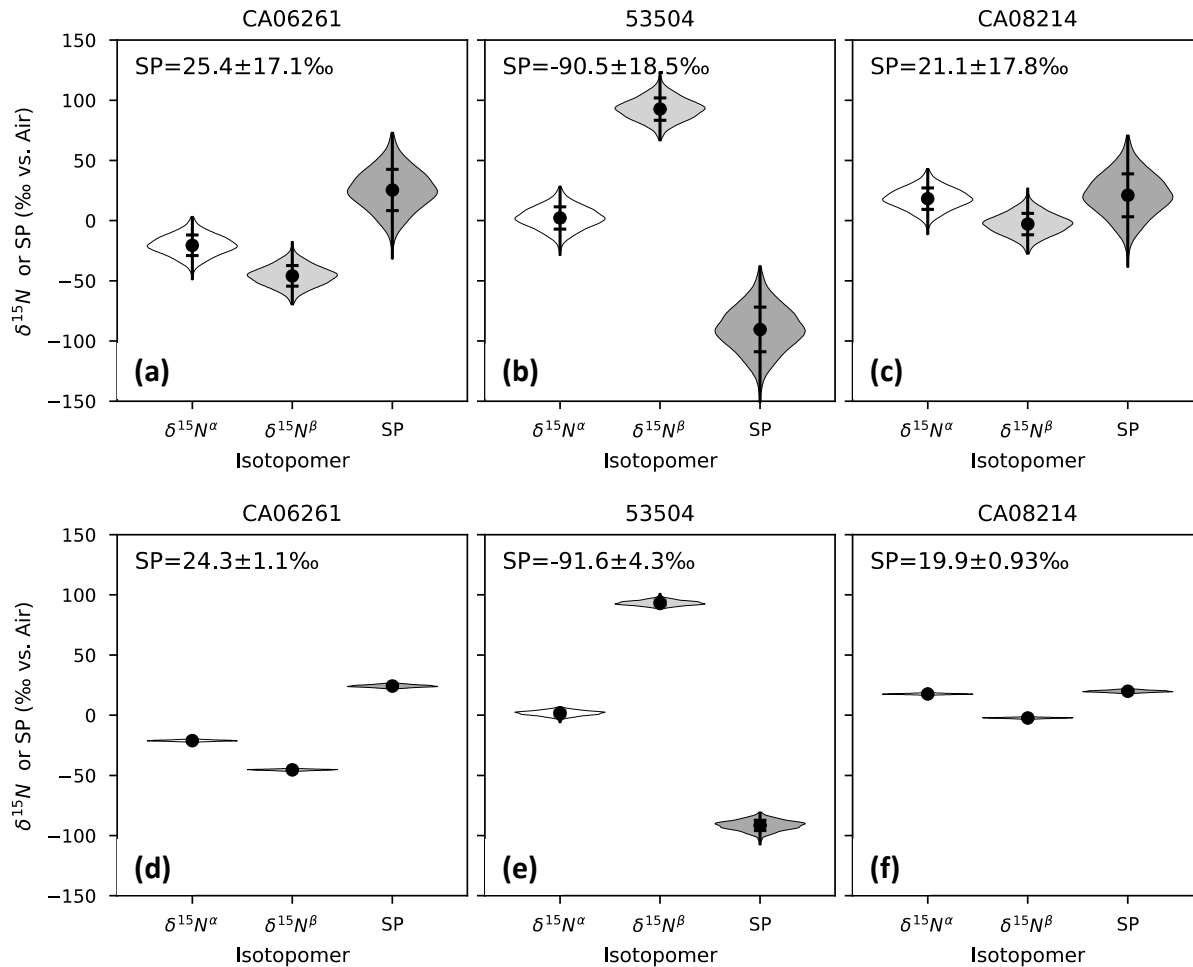
990



991 **Figure 3.**  $\gamma - \kappa$  for the Lab 1 IRMS from June 2018 to March 2021. Daily mean  $\gamma - \kappa$  (black line) values are plotted  
 992 with a 5-day rolling average (dots).  
 993

994





995  
 996 **Figure 4.** a-c) Isotopocule values and error associated with a 10 % relative uncertainty in  $\gamma - \kappa$ , based on Monte  
 997 Carlo simulation results, for reference materials CA062621 (a), 53504 (b), and CA08214 (c).  $\gamma$  and  $\kappa$  were modeled  
 998 as random numbers centered around  $\gamma = 0.174$  and  $\kappa = 0.083$ , with the uncertainty in  $\gamma - \kappa$  equal to 10 % of the mean  
 999  $\gamma - \kappa$  (0.091). d-f) Isotopocule values and error associated with a 10% relative uncertainty in the absolute values of  $\gamma$   
 1000  $- \kappa$ , holding the difference  $\gamma - \kappa$  constant, for reference materials CA062621 (d), 53504 (e), and CA08214 (f).  $\gamma$  and  
 1001  $\kappa$  were modeled in tandem as random numbers centered around  $\gamma = 0.174$  and  $\kappa = 0.083$ , with uncertainties equal to  
 1002 10% of the mean  $\gamma$ , and  $\gamma - \kappa$  was held constant at 0.091. Violin plots are based on a kernel density estimate of the  
 1003 distribution and the values plotted and reported on each figure show the mean value  $\pm 1\sigma$ .

1004  
 1005  
 1006  
 1007